AFRL-RH-WP-TR-2019-0085

Computational Airflow Models to Evaluate Biological Agent Transport in Cargo Aircraft

Daniel Reilly, MS
Christin Duran, PhD

December 2019

Final Report
for February 2019 to July 2019

Air Force Research Laboratory
711HPW/RH
2510 Fifth St., Bldg. 840
Wright-Patterson AFB, OH 45433-7913

NOTICE AND SIGNATURE PAGE

Using Government drawings, specifications, or other data included in this document for any purpose other than Government procurement does not in any way obligate the U.S. Government. The fact that the Government formulated or supplied the drawings, specifications, or other data does not license the holder or any other person or corporation or convey any rights or permission to manufacture, use, or sell any patented invention that may relate to them.

Qualified requestors may obtain copies of this report from the Defense Technical Information Center (DTIC) (http://www.dtic.mil).

AFRL-RH-WP-TR-2019-0085 HAS BEEN REVIEWED AND IS APPROVED FOR PUBLICATION IN ACCORDANCE WITH ASSIGNED DISTRIBUTION STATEMENT.

//SIGNATURE//	//SIGNATURE//
Name	Name
TAMERA G. BORCHARDT, Lt Col, NC	GUY R. MAJKOWSKI, Col, BSC
Branch Chief, Biomedical Impact of Flight	Division Chief, Warfighter Medical Optimization

This report is published in the interest of scientific and technical information exchange, and its publication does not constitute the Government's approval or disapproval of its ideas or findings.

REPORT DOCUMENTATION PAGE

Form Approved
OMB No. 0704-0188

1. REPORT DATE *(DD-MM-YYYY)*	2. REPORT TYPE	3. DATES COVERED *(From – To)*
01-12-2019	Final	February 2019 to July 2019

4. TITLE AND SUBTITLE
Computational Airflow Models to Evaluate Biological Agent Transport in Cargo Aircraft

5a. CONTRACT NUMBER

5b. GRANT NUMBER

5c. PROGRAM ELEMENT NUMBER

6. AUTHOR(S)
Daniel Reilly, Christin Duran

5d. PROJECT NUMBER
17-077

5e. TASK NUMBER

5f. WORK UNIT NUMBER

7. PERFORMING ORGANIZATION NAME(S) AND ADDRESS(ES)
Medical Optimization Division
Airman Readiness Optimization Branch
2510 Fifth St., Bldg. 840
Wright-Patterson AFB, OH 45433-7913

8. PERFORMING ORGANIZATION REPORT NUMBER
AFRL-RH-WP-TR-2019-0085

9. SPONSORING / MONITORING AGENCY NAME(S) AND ADDRESS(ES)

10. SPONSORING/MONITOR'S ACRONYM(S)

11. SPONSOR/MONITOR'S REPORT NUMBER(S)

12. DISTRIBUTION / AVAILABILITY STATEMENT
DISTRIBUTION STATEMENT A. Approved for public release. Distribution is unlimited.

13. SUPPLEMENTARY NOTES
Cleared, 88PA, Case # 88ABW-2019-6168, 30 Dec 19

14. ABSTRACT

There is currently a lack of real-world data and computational models aimed at characterizing Air Force cargo aircraft cabin ventilation. A better understanding of the flow physics could be used to identify hot spots where contaminants introduced into the aircraft are likely to accumulate, which would inform sampling strategies to confirm decontamination after an incident. Further, an in-depth flow understanding could be used to improve strategies for infectious patient transport to mitigate cross-contamination. In the absence of available data, a set of numerical Lagrangian Multiphase aerosol transport models were completed to investigate various flow and aerosol metrics in a C-130 cabin outfitted for aeromedical evacuation. The transport properties, including residence time, deposition and clearance of 100,000 polydispersed (0.1, 1.0, 10.0 μm) expiratory particles that mimicked wet microorganism-bearing droplets were examined in four distinct models in which aerosolization occurred at different time points (1, 41, 81, 121 s). In each model, the simulated bioaerosols were released from the same single location and tracked for up to three minutes. Simulation results were investigated in the following manner: air velocity and direction on cut planes throughout the cabin, randomly sampled particle trajectories, particle deposition rates, particle deposition location binning and particle maximum velocities. Cabin air exhibited a combination of positive and negative forward to aft flow in the cabin which fluctuated in time. Analysis of single-particle trajectories revealed low travel distance from the point of expiration with the particles being continually re-entrained into rotating vortices in the flow. The highest rates of deposition occurred directly following each expiration; however, the majority of all particles (70% on average) remained suspended in vortices for the duration of the simulations. A small percentage of particles cleared the cabin through the ventilation outlets (23% on average) and only 6% of the particles deposited to cabin surfaces on average. Deposition patterns were consistent across all four models in which particles primarily deposited on surfaces nearest the expiration point. Particles adhered to the cabin sidewalls more often than any other surface (58%), followed by the cargo floor (27%). The 10 μm particles were 1.5 times more likely than the 0.1 and 1.0 μm particles to settle on horizontal surfaces. Finally, particles entrained into higher-speed flow vortices were less likely to deposit or settle on surfaces. Follow-on efforts to validate these results will be executed via aerosol sampling methods aboard operational C-130 aircraft.

15. SUBJECT TERMS
Computational Fluid Dynamics, Aerosol Transport Modeling, Aeromedical Evacuation, Disease Transmission, Decontamination

16. SECURITY CLASSIFICATION OF:			17. LIMITATION OF ABSTRACT	18. NUMBER OF PAGES	19a. NAME OF RESPONSIBLE PERSON
a. REPORT	b. ABSTRACT	c. THIS PAGE			Christin Duran
U	U	U	SAR	31	19b. TELEPHONE NUMBER *(include area code)*

This page intentionally left blank.

TABLE OF CONTENTS

Section **Page**
LIST OF FIGURES ii
LIST OF TABLES ii
ACKNOWLEDGEMENTS iii
1.0 EXECUTIVE SUMMARY 1
2.0 INTRODUCTION 2
3.0 APPROACH 4
3.1 Domain Geometry Development 4
3.2 Boundary Conditions 5
3.3 Computational Grid 6
3.4 Physics Setup and Solvers 7
3.5 Study Design 8
4.0 RESULTS 9
4.1 Unsteady Flow Structures 9
4.2 Particle Tracing 11
4.3 Suspended Particulate Velocity Metrics 12
4.4 Particle Deposition 13
5.0 DISCUSSION 16
6.0 CONCLUSIONS AND FUTURE WORK 17
REFERENCES 19
ABBREVIATIONS 21
APPENDIX A 22
APPENDIX B. 23
APPENDIX C 31

LIST OF FIGURES

Page
Figure 1 – C-130 exterior and interior 4
Figure 2 – Finalized CAD model of the cabin geometry from three perspectives 5
Figure 3 – Ventilation system boundary conditions throughout the aircraft 6
Figure 4 – Computational mesh near the patients 7
Figure 5 – Computational mesh at ventilation inlet and outlet boundary condition locations 7
Figure 6 – Cough profile for particle injections 8
Figure 7 – Derived surface parts used to visualize flow 9
Figure 8 – Air velocity in forward to aft direction on plane 6 in model 1 at four time points 10
Figure 9 – Air velocity in forward to aft direction on planes 1-5 in model 1 at four time points 11
Figure 10 – Particle position tracking visualization 12
Figure 11 – Maximum particle velocity (Vmax) in time 13
Figure 12 – Number of airborne particles suspended in the simulation over time 14
Figure 13 – Number of particles which adhered to each surface of interest 16
Figure A1 – C-130 point cloud scan locations 22
Figure A2 – Fully registered software-generated C-130H point cloud 22
Figure B1 – Air velocity in forward to aft direction on plane 6 in model 2 23
Figure B2 – Air velocity in forward to aft direction on plane 6 in model 3 24
Figure B3 – Air velocity in forward to aft direction on plane 6 in model 4 25
Figure B4 – Air velocity in forward to aft direction on plane 1 in models 1-4 26
Figure B5 – Air velocity in forward to aft direction on plane 2 in models 1-4 27
Figure B6 – Air velocity in forward to aft direction on plane 3 in models 1-4 28
Figure B7 – Air velocity in forward to aft direction on plane 4 in models 1-4 29
Figure B8 – Air velocity in forward to aft direction on plane 5 in models 1-4 30
Figure C1 – Detailed particle deposition patterns by mass for each of the four models 31

LIST OF TABLES

Table 1 – Particle Fate 50 Seconds Post Initial Deposition 15

ACKNOWLEDGEMENTS

This work would not have been possible without support from MSgt Garrett Medley with USAFSAM/ETT who provided RHMO researchers access to a training C-130 aircraft to scan the cabin geometry. The simulations were completed via a subcontract with Siemens AG (Germany).

1.0 EXECUTIVE SUMMARY

There is currently a lack of published models or data characterizing airflow movement within Air Force (AF) cargo aircraft. A better understanding of airflow movement could be used to identify hot spots where biological aerosols are likely to accumulate, which would inform sampling strategies to confirm decontamination after an incident. Further, it could be used to improve strategies for infectious patient transport to mitigate cross-contamination and passenger-to-passenger disease transmission. In the absence of available data, a set of computational fluid dynamic (CFD) aerosol transport models were completed to investigate various airflow and aerosol metrics in a C-130 cabin outfitted for aeromedical evacuation (AE).

CFD models were generated and evaluated using a computational continuum mechanics software package, STAR-CCM+ (Siemens AG, Germany). Airflow in the absence of an aerosol was simulated first, employing standard ventilation system cabin inlets and outlets. The simulation revealed transient flow dynamics. To evaluate aerosol transport in transient flow, 100,000 particles in three size ranges (0.1, 1.0, 10 μm) were aerosolized using a published cough profile at four time points including 1, 41, 81 and 121 s in four distinct models. Simulation results were investigated in a variety of manners including: air velocity direction from forward to aft on six cut planes throughout the cabin, randomly sampled particle trajectories, particle deposition rates, particle deposition patterns and maximum particle velocities.

Model results indicated that cabin airflow exhibited a combination of positive and negative flow from forward to aft which fluctuated in time. Aerosol movement investigated using single-particle trajectories revealed low travel distance from the point of expiration. This occurred due to the aerosol being continually re-entrained into rotating vortices in the flow, indicating that airflow dominated particle transport. The highest rates of deposition occurred directly following each expiration; however, the majority of all particles (70% on average) remained suspended for the duration of each simulation. A smaller percentage cleared the cabin through the ventilation outlets (23% on average), and only 6% of the particles deposited to cabin surfaces on average.

Deposition patterns were consistent across all four models in which the surfaces nearest the expiration experienced the greatest deposition magnitudes. This indicated that regardless of transient flow physics, the point in time when the particles were released did not strongly impact particle deposition. Particles adhered to the cabin sidewalls more often than any other surface (58%) followed by the cargo floor (27%). The 10 μm particles were 1.5 times more likely than the 0.1 and 1.0 μm particles to settle on horizontal surfaces. Finally, deposition rates and maximum particle velocity correlated, indicating the particles entrained into higher-speed flow vortices were less likely to deposit or settle on a surface.

The results of this study demonstrate a proof-of-concept simulation for the distribution of aerosols of biologically relevant size and density aboard a military cargo aircraft. Several of the observations agree with published results in civilian passenger aircraft mock-up simulations, including the dominance of bulk airflow on particle transport for small particles (≤ 10 microns) and the effect of increased airflow velocity resulting in decreased particle deposition for particles in this same size range. However, the airflow patterns themselves are unique in military aircraft compared to civilian aircraft. Therefore, follow-on studies are required to validate computational predictions. Validated computational models of airflow in AF cargo aircraft will be invaluable for guiding bioaerosol sampling methodologies and AE infectious patient transport strategies.

2.0 INTRODUCTION

Airflow patterns and bioaerosol transport aboard aircraft are important to understand due to the role they play in disease transmission. In both commercial and military aviation applications, large numbers of passengers are transported in a confined compartment while seated in close proximity for many hours at a time. In civilian aircraft, the expirations from sick and infectious passengers have been shown to form a pathogen-containing mist which has been predicted to travel for prolonged periods through air currents, providing the recurrent opportunity for nearby passenger inhalation (Gupta et al., 2010). This phenomenon is of particular interest to the AF AE community due to their primary mission to provide medical care, support, treatment, staging and transport of sick and infected patients.

Wet microorganism-bearing droplet aerosols can be generated from a range of expiration events, including coughing, sneezing, breathing and talking (Fernstrom and Goldblatt, 2013; Stelzer-Braid, 2009). These wet droplets and droplet nuclei vary in size from < 1.0 up to 1000 μm (Chao et al., 2009; Fabian et al., 2008; Lindsley et al., 2010; Morawska et al., 2009). The transport properties of droplets and droplet nuclei in indoor environments depend on aerodynamic diameter and local airflows (Morawska, 2006). Droplets and droplet nuclei < 20 μm have been shown to travel for prolonged periods of time in airflows, so are of particular interest in regards to disease transmission.

Airborne droplet concentration is a key factor in the number of susceptible people in a given space and increases when the aerosol generation rate is high and air exchange rates are low (Nardell, 1990). Aerosol generation rate has the potential to be extremely high in an AE scenario where up to 74 infected patients are being transported at once (Crowhurst, 2011). Higher air exchange rates are generally recommended to remove infectious biological aerosols for cases with infectious patients. For instance, it is recommended that hospital isolation rooms of patients with active tuberculosis receive ≥ 12 air exchanges per hour (for new construction since 2001) compared to a normal home environment which is generally between zero and two (CDC, 2005; Frankel et al., 2012). Air exchange rates aboard aircraft vary widely with manufacturer, ranging from 6 to 26 exchanges per hour (Withers, 2000; Hocking, 1998). As such, proper confidence in ventilation efficiency and air exchange rate is on an airframe-to-airframe basis and has spurred many investigative studies, primarily in commercial applications.

The common flow structure in commercial passenger transport aircraft consists of two counter-rotating vortices running the length of the aircraft (Elmaghraby et al., 2018). The aircraft ventilation systems includes inlets at the top of the cabin and flow outlets near the passengers' feet under the window seats, both running the length of the cabin. This design is common due to the flow effect which ideally limits the row-to-row air transport, keeping flow in the same aircraft cross-section for its duration in the cabin. It should be noted that military aircraft used for AE such as the C-130 do not employ the same ventilation system design considerations as the passenger seats and patient stretchers are designed to be easily reconfigured based on mission requirements (Crowhurst, 2011).

Experimental investigation of particle movement throughout commercial airframes have been performed to investigate particle flow using a combination of particle image velocimetry, interferometric mie imaging and direct measurement through airborne particle counters and sizers (Sze To et al., 2009; Zhai et al., 2014). Sze To et al. (2009) conducted a comprehensive study using particle image velocimetry and interferometric mie imaging to investigate airflow effect on cough particle dispersion and deposition in a Boeing 767 mockup, concluding that an

aerosol emitted from a passenger located near the sidewall of an aircraft could reach the breathing zone of passengers two rows away within 30 s. This indicated the counter-rotating vortex ventilation design was efficient, but not perfect. Further, the study showed that up to 70% of the aerosol mass was deposited suggesting a further avenue for direct disease transmission through physical contact. A similar experimental study examined the effect of ventilation system parameters on particle concentrations in cabin air supply and return during nine 737 flights (Zhai et al., 2014). Air exchange rates were analyzed in concurrence with measured particle size from human emission in which results indicated deposition occurred little for particles smaller than 5.0 μm, and air exchange rate and human emission rate had the strongest impact on suspended particles smaller than 2.0 μm.

In addition to experimental studies, numerical models have been developed focused directly on expiratory aerosols and their associated infection risk (Wan et al., 2009; Gupta et al., 2010). Wan et al. (2009) used a Lagrangian-based numerical model in an aircraft cabin mockup to show that aerosol deposition fraction increased with aerodynamic diameter, and passengers were two orders of magnitude more likely to be subject to contact risks when sitting within one row of the location of aerosol expiration. In similar work, exhaled droplet dispersion was simulated in a seven-row section of a twin-isle aircraft (Gupta et al., 2010). Results showed that droplet movement was governed by bulk airflow after the initial discharge and droplets followed similar trajectories independent of discharge time, indicating that suspended particles from different discharges could accumulate in the same flow structures with periodic exhalations.

Additional studies exhibiting similar results have been conducted using a combination of experimental and numerical techniques used in parallel, ensuring validated numerical results. Gupta et al. (2011a, 2011b) conducted a series of comprehensive studies in which expiratory droplet aerosolization, their subsequent inhalation by nearby passengers and the resulting airborne risk of infection was investigated. Three expiratory events were simulated using the methods including breathing, coughing and talking, with uniform aerosol droplet sizes of 0.4, 8.5 and 30 μm, respectively. Results indicated that expiration aerosol movement was initially governed by the cough jet and subsequently by the bulk cabin flow. Further, assuming the particles were perfectly mixed after three minutes resulted in a numerical/analytical correlation with less than 10% difference.

The use of these aforementioned experimental methods and computational simulations have yet to be applied to characterize airflow and aerosol transport in military aircraft designed for AE, such as the C-130 (see Fig. 1A). While the results from commercial studies can be useful in gaining insight into what may be happening in military aircraft, there are distinct differences that warrant further investigation. For example, commercial passenger aircraft are generally designed with many rows of stationary seats which create a natural flow buffer, creating a scenario in which passengers are for the most part only exposed to exhalations of the passengers sitting within a few rows. On the contrary, military cargo aircraft outfitted for AE are designed with several stanchions that hold litters for patients with no natural barriers blocking flow from moving in the positive and negative forward to aft directions. Further, passengers are often lying flat in a recumbent position in contrast to being seated, and other cargo such as patient support palates can be variably assembled, dependent on operational needs (Fig 1B) (Crowhurst, 2011). The ventilation systems in military aircraft are not designed specifically for low flow movement and as such, these differences have the potential to play a large role in how expiratory aerosols are transported.

A. B.

Figure 1 – C-130 exterior and interior
A. C-130 airframe (photo credit – U.S. Air Force, 2013);
B. Typical AE litter format and spacing (photo credit – U.S. Air Force, 2011).

In the present study, CFD was used to model air flow and aerosol transport and fate in a mock military aircraft cabin modelled after the C-130 Hercules (Fig. 1). The aircraft cabin geometry was generated using a combination of laser-scanning techniques and computer aided design. Particles in the size range 0.1, 1.0 and 10 μm were aerosolized using a previously published cough profile in four distinct models where particles were released at four different time points including 1, 41, 81 and 121 s. The simulation output was investigated to evaluate the effect of particle release time on transport and fate in the aircraft cabin. Results will be validated in follow-on studies. Ultimately, validated computational models of military cargo aircraft will be useful for designing biological agent sampling and decontamination strategies and updating guidance for infectious patient transport operating procedures.

3.0 METHODS

3.1 Domain Geometry

The domain geometry was developed using a combination of laser scanning technologies and computer aided design (CAD) software. A portable laser scanner (Faro Focus M70, FARO Technologies, Lake Mary, FL) was employed to capture a point cloud within a C-130H used for AE training. The device contains a laser with a combination of motors and a spinning mirror to capture 360-degree line-of-sight geometry data on two rotational axes, resulting in a three-dimensional point cloud of the surrounding volume. Additional sensor data included an inclinometer, compass, altimeter and GPS which aided in the multi-scan registration process post collection. Sixteen unique scans at varying locations throughout the cabin were collected using a standard indoor laser profile. The laser scanner output from each scan was processed and registered to a single point cloud in the corresponding software, SCENE Version 2018.0.0.648 (FARO Technologies, Lake Mary, FL). Registration resulted in a point cloud with maximum point error being less than 19 mm and mean point error being less than 7.5 mm, indicating that the combination of scans was accurate (see Appendix A).

Geometric dimensions were then derived using the point cloud developed from the scan in order to generate a CAD file of the C-130H cabin in Solidworks 2018 (Dassault Systems, France). The CAD file consisted of a combination of surfacing functions including surface-extrude, surface-trim, surface-plane and surface-knit. The point cloud was used to take virtual

measurements of the domain and create an analogous solid model. The length of the cabin including the flight deck, cargo door and cargo bay measured nearly 79 ft, the width of the cabin measured slightly greater than 13 ft, and the height measured nearly 12 ft, which correlates well with expected measurements (Lockheed Martin). Detailed measurements were gathered from the point cloud for the ventilation system inlets and applied in the CAD development. Intricate detail such as the bulkheads, wiring and storage compartments were disregarded and assumed to have little effect on CFD results. The "hell hole", which is a space underneath the flight deck, was not included in the cabin volume. Ten identical patient and litter geometries were added to the cabin volume in two columns of five patients distributed throughout the cabin at approximately hip-height to represent an AE-4 scenario based on the Air Force Instruction 11-2AE Volume 3, Addenda-A (Crowhurst, 2011).

The Solidworks CAD model was exported as a Parasolid binary file (.x_b), a geometric modeling kernel owned and licensed by Siemens Product Lifecycle Management, which allowed the file to be ported as Parts and Surfaces into CFD software (STAR-CCM+, Siemens AG, Germany). The single cabin Part was subsequently split into Surfaces including the cargo door, cargo bay floor, ventilation inlets and outlets and main fuselage to make boundary condition application and locational particle deposition investigation possible. Similarly, each of the patient Parts were split into two Surfaces including the patient and litter. The root Part meshes were then repaired for self-intersection, invalid geometry, overlapping entities, topology errors and non-manifold geometry in an effort to create the single airtight volume necessary for CFD. Three views of the completed Part file can be seen in Figure 2.

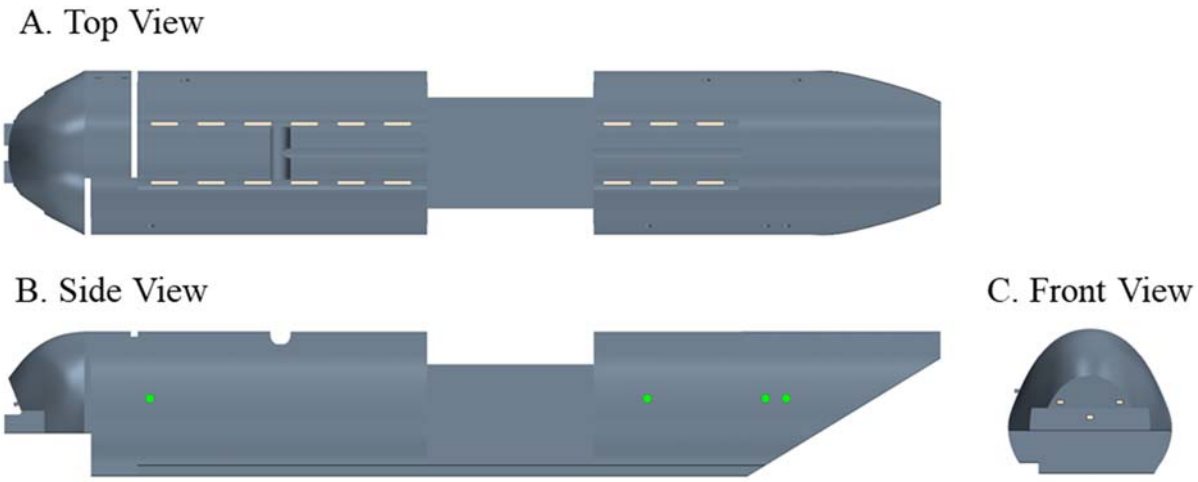

Figure 2 – Finalized CAD model of the cabin geometry from three perspectives A. Top; B. Side; C. Forward.

3.2 Boundary Conditions

A total of eighteen oblong shaped ventilation inlets spanned the length of the cargo bay at regular intervals along the ceiling of the cabin (Fig 3A). These inlets were 1.7 ft long and 0.25 ft wide. Five ventilation inlets were dispersed throughout the flight deck and were of dimensions 0.42 ft wide and 0.25 ft tall (Fig 3B). Airflow was assumed to enter the cabin through the twenty-three inlets perpendicularly to their surface at a total mass flow rate of 160 lb/min which

correlated to a complete air exchange every 99.3 s. The mass flow rate value was provided as an estimate by the AC-130J System Program Office. Airflow was assumed to exit the cabin at a comparable flow rate through seven vents along the fuselage (Fig 3C).

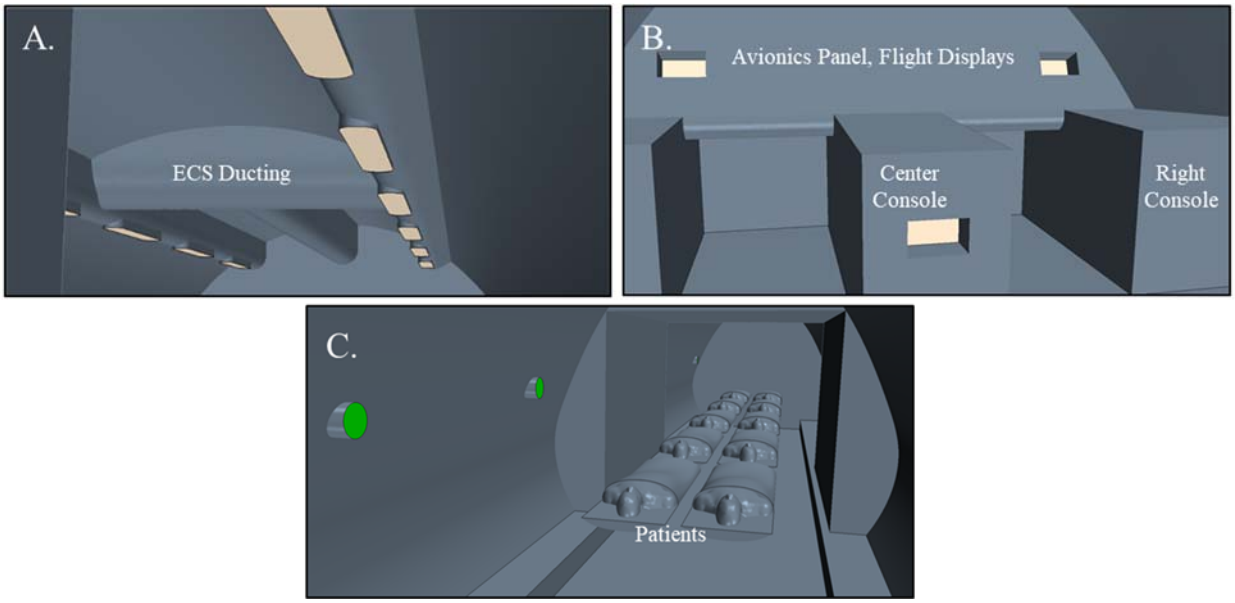

Figure 3 – Ventilation system boundary conditions throughout the aircraft
A. Overhead ventilation inlets in the cargo bay; B. Ventilation outlets; C. Ventilation inlets in the flight deck.
***ECS = Environmental Control System**

3.3 Computational Grid

The cabin volume was discretized employing polyhedral mesh elements in a uniform manner throughout (Fig 4A). A polyhedral mesh shape was employed due to its affinity for resolving recirculating flows accurately. This cell shape has significantly more neighboring cells than hexahedral or tetrahedral elements, so gradients can be much better approximated using linear shape functions and information from neighboring cells even with a smaller total cell count. The single downside being that more neighboring cells requires more storage during compute operations.

A prism layer model was used in conjunction with the core polyhedral mesh to ensure flow resolution near the surfaces was accurate, a critical step when predicting aerosol accumulation patterns on surfaces (Fig 4B). Orthogonal prismatic cells were generated on all cabin, patient and litter surfaces excluding the boundary condition inlets and outlets. As velocity and temperature gradients are much steeper in the viscous sublayer of a turbulent boundary layer, such a method ensures proper wall treatment, a set of assumptions for accurately approximating near-wall turbulent production, dissipation and shear stress. These cells provide higher near-wall density as well as high aspect ratio cells which results in better cross-stream resolution and numerical diffusion reduction near the wall, a discretization error that smears discontinuities and steep gradients in a finite volume advection scheme.

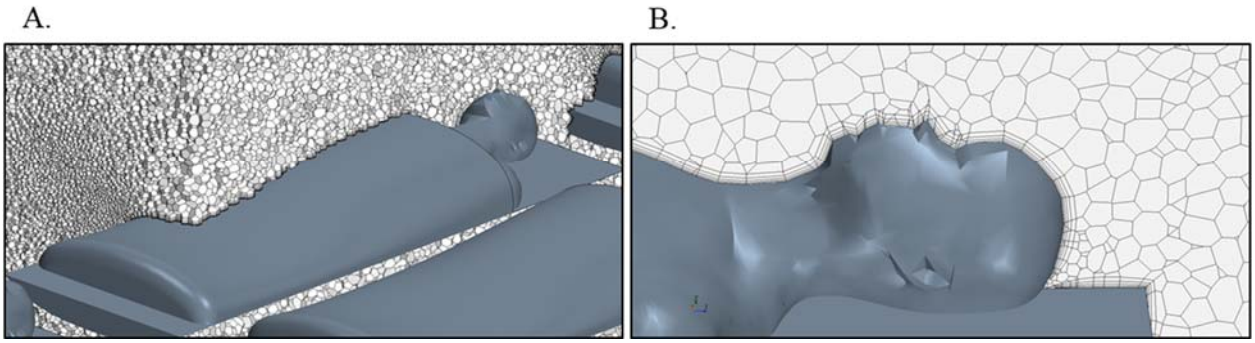

Figure 4 – Computational mesh near the patients
A. 3d representation of the mesh surrounding a patient and litter; B. 2d view showing a patient face with prism layers along its surface.

The total cell count used for all simulations was 10.3M. The mesh operation employed surface repair and re-mesher in addition to the polyhedral and prism layer meshers. Element reference length, the initial size constraint for a single element, was 0.09 ft. Five prism layers with a 1.5 stretch ratio and a total thickness of 0.033 ft were generated on all physical surfaces. A custom surface size constraint of 0.01 ft was implemented on all inlet and outlet boundary conditions in order to ensure high-fidelity upon flow onset (Figs 5A and 5B). The surface growth rate ratio was 1.25 throughout. Cell quality remediation and proximity interpolation were employed to ensure mesh quality.

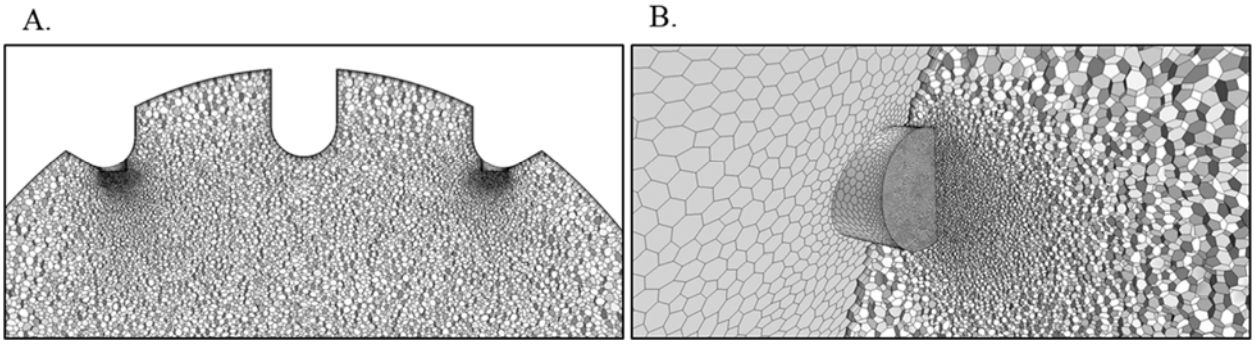

Figure 5 – Computational mesh at ventilation inlet and outlet boundary condition locations
A. 3d representation of extra refinement on inlet boundary conditions; B. 3d representation of extra refinement on an outlet boundary condition.

3.4 Physics Setup and Solvers

All simulations employed an implicit unsteady Reynolds Averaged Navier-Stokes scheme with a 0.05 s time-step and a first-order temporal discretization. The gas was treated as ideal and as such the segregated (uncoupled) flow solver was used, meaning the link between mass and momentum was achieved through a predictor-corrector approach. Segregated solvers have roots in constant-density flows. A shear stress transport (SST Menter) K-Omega turbulence model was used, in which two transport equations were solved for turbulent kinetic energy (k) and specific dissipation rate (omega) for turbulent eddy viscosity. Gravity was set to 32.2 ft/s^2 in the direction of the aircraft floor.

Aerosol physics was predicted using a Lagrangian Multiphase model. Multiphase models are used to simulate scenarios where a mixture of phases are present simultaneously in the same fluid domain (i.e. aerosol and air). Aerosols of three different aerodynamic diameters were included in the simulation and treated as three unique phases. The aerosol was treated as material (not massless) spherical particles with a Schiller-Naumann drag force coefficient. Specific aerosol metrics that were stored during computation for post-processing included: track files for single particle position and velocity in time, boundary sampling and parcel depletion to evaluate escaped particle numbers and residence time for particle duration in the domain. Particles were modeled as liquid with a constant density material property of water (62.3 lb./ft^3), meaning the particles with larger aerodynamic diameter had a larger mass. An assumption was made that particle-particle interaction would be insignificant to bulk deposition and accumulation patterns.

3.5 Study Design

Preliminary simulations focusing only on airflow physics (no aerosols) showed unsteady flow structure undulation throughout the cabin. In order to investigate the effect of the flow's temporal variation, undulation and direction on aerosol residence time and deposition patterns, four distinct models were executed with identical geometry, boundary conditions and aerosol physics. The single difference between the four models was the point in time at which the 1.2 s particle expiration occurred. The expirations occurred at 1 s, 41 s, 81 s and 121 s in models 1, 2, 3 and 4, respectively.

The particles were injected a single time per model using a common human cough pattern in which the flow rapidly peaked after approximately 0.2 s and trailed off over a period of 1 s (Fig. 6). The cough profile exhibited a total volume of 4.16 L, a peak velocity of 33.5 ft/s and a peak flow rate of 11.1 L/s to represent realistic conditions as measured by Lindsley and colleagues (2013).

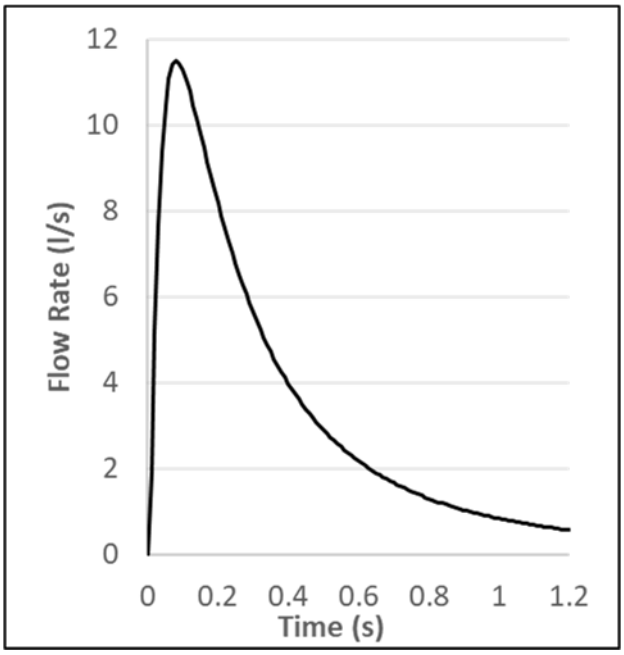

Figure 6 – Cough profile for particle injections
Data plotted from source – Lindsley et al. 2013.

Exhalation injections, directed towards the aircraft aft, occurred along the centerline of the aircraft at a location 3 ft from the forward bulkhead at a height of 5 ft. Exhalation injections into the simulation occurred at 1, 41, 81 and 121 s for models 1, 2, 3 and 4, respectively. Injection times were chosen accounting for the time in which planned validation devices require to generate the pseudo cough. Each injection included a phase for each of the three aerodynamic diameters (0.1 µm, 1.0 µm, 10 µm) with particle counts of 33,333 for each phase. These three diameters were chosen because they are within the size range of greatest concern in disease transmission. Particulate parameters included a no bounce, stick wall interaction condition to simulate wet droplet deposition and adherence in which it was assumed no re-aerosolization occurred. Droplet density was 62.28 lb/ft^3, equivalent to water. Particle indices and tracks were visualized within STAR CCM+ software.

4.0 RESULTS

4.1 Unsteady Flow Structures

Flow was investigated and visualized on six planes throughout the aircraft cabin, with the majority being concentrated at locations near the forward bulk head surrounding the location in which particles were injected. Cut planes 1-5 were parallel to the forward bulkhead and occurred at 2 ft increments (Fig. 7). Cut plane 6 was perpendicular to the forward bulkhead and bisected the airframe. Flow was primarily investigated on these planes for positive forward to aft velocity magnitude and direction, in this case the $\hat{k}$ component of the velocity vector magnitude. Three-component ($\hat{\imath}, \hat{\jmath}, \hat{k}$) velocity magnitudes were in the 5.0 ft/ range with the bulk of that in the -$\hat{\imath}$ (top to bottom) direction.

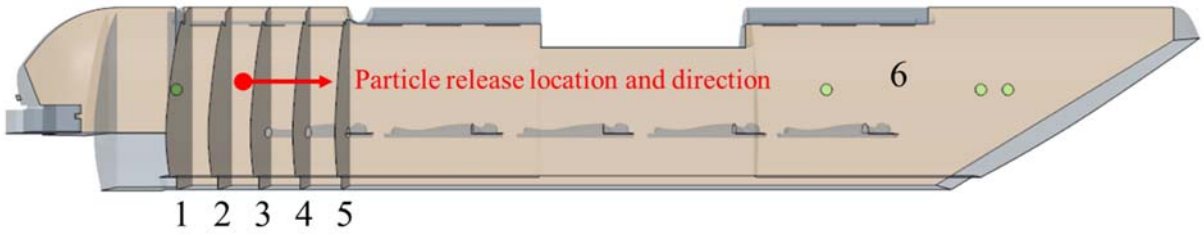

Figure 7 – Derived surface parts used to visualize flow

Four 12 s blocks of time starting 9-19 s after the expiration event for each of the four models were scrutinized due to their association with high frequency particle deposition. Initial investigation of the 12 s time block in model 1 (20 s to 32 s) in 4 s increments on plane 6 showed the vast majority of the flow moving from forward to aft (Fig. 8, positive flow, red) at a magnitude between 0.0 and 0.5 ft/s; however, it was common for localized occurrences of k-component flow moving from aft to forward (Fig. 8, negative flow, blue) at similar magnitudes. The center portion of the cargo bay, starting at Plane 5 and continuing past the patients towards the aircraft aft, exhibited the highest magnitudes of positive flow throughout the 180 s simulations. Flow was most commonly in the negative direction (aft to forward) in the 9 ft span starting from the forward bulkhead. Patients and their litters seemed to have minimal immediate effect on bulk flow development.

The flight deck proved to exhibit a combination of positive, stagnant and negative flow with the majority of the positive flow resulting directly from the ventilation inlets. Negative flow occurred consistently near the ceiling of the flight deck. Flow was nearly stagnant in a large portion of the volume surrounding the cargo door. General trends in positive and negative flow along plane 6 were carried throughout the entirety of the 180 s simulations for each of the four models. Similar snapshots for 12 s time blocks for models 2, 3 and 4 beginning at 50, 90 and 130 s, respectively are included in Appendix B (Figs. B1-B3).

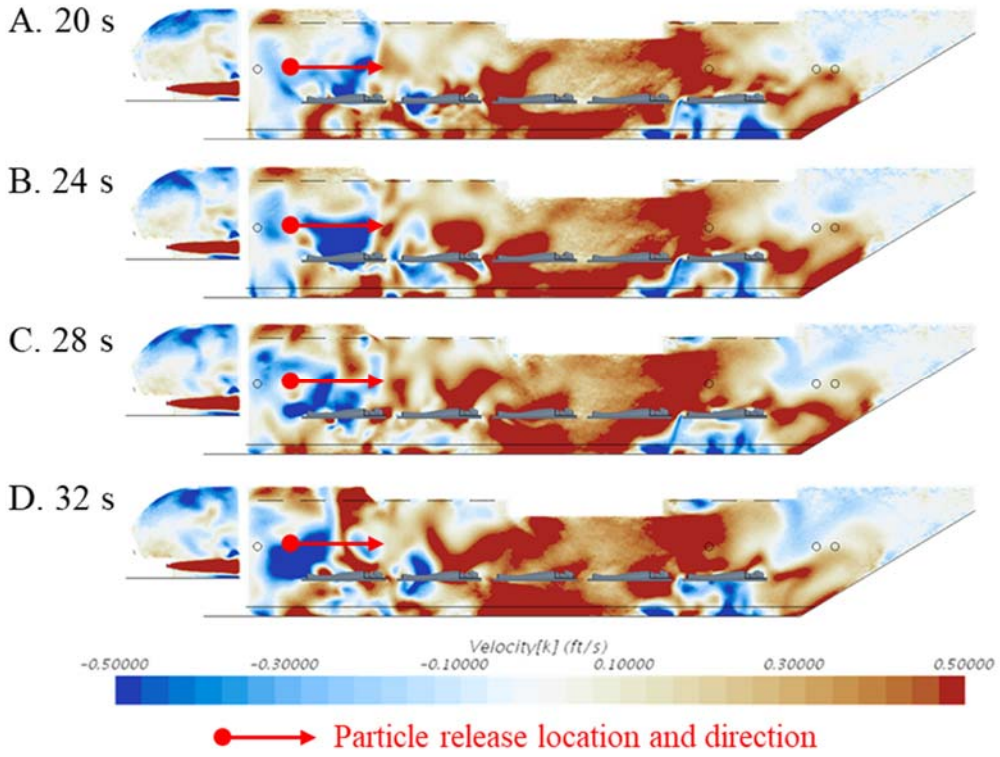

Figure 8 – Air velocity in forward to aft direction on plane 6 in model 1 at four time points A. Flow at 20 s snapshot; B. Flow at 24 s snapshot; C. Flow at 28 s snapshot; D. Flow at 32 s snapshot.

Planes 1-5 showed similar results along cut planes perpendicular to plane 6 and parallel to the forward bulkhead (Fig. 9). Flow was perceived to exhibit transient flow structures in a combination of positive and negative flow. Flow direction variation was high in all temporal and locational snapshots, however negative flow was more commonly observed at the center of planes 1-5 and along the floor of the aircraft whereas positive flow occurred around the perimeter of the same cut planes.

Plane 1 showed the least temporal variation of the five planes with consistent positive flow at the side walls, negative flow near the cargo floor and a mix of positive and negative near-stagnation flow in the center of the geometry (Fig 9). A section along the upper portion of the left sidewall of plane 2 showed constant positive flow. Solutions on plane 3 exhibited similar tendencies with highly negative flow near the center of the geometry at 28 and 32 s; however, in contrast to plane 2, the flow direction on the section along the upper portion of the left sidewall was negative. Counter-rotating vortices developed on plane 3 with flow originating from the

overhead inlets and circling back to the top along the aircraft sidewalls. Plane 4 showed positive flow between the ventilation inlet jets with the exception of a periodic negative gust just over the patient litters which developed at 20 s and shed just after 24 s. Plane 5 showed the most variation in flow direction, nearing the point (approximately 9 ft from the forward bulkhead) at which the flow was highly negative dominated to highly positive dominated. Similar snapshots for 12 s time blocks for all four models on each plane (1-5) are included in Appendix B (Figs. B4-B8).

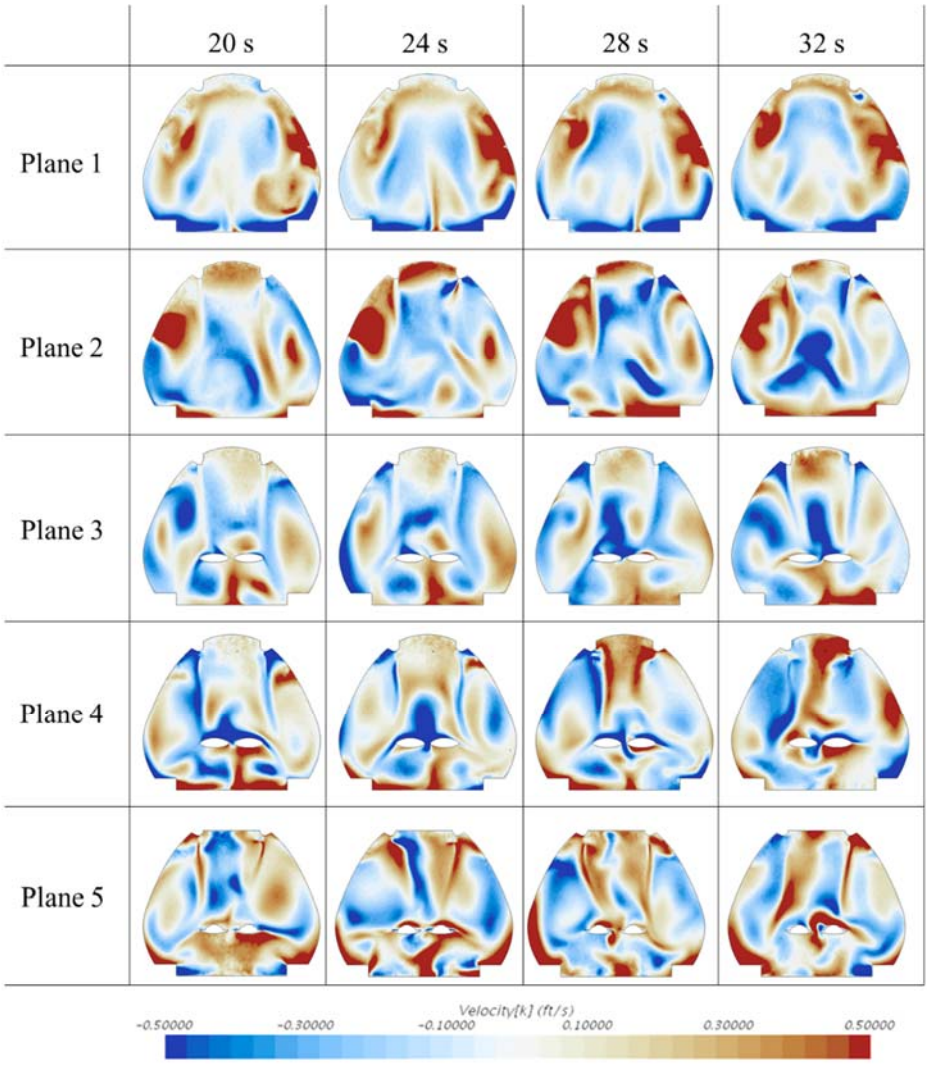

Figure 9 – Air velocity in forward to aft direction on planes 1-5 in model 1 at four time points

4.2 Particle Tracing

All of the approximately 100,000 particles per expiration were tracked while airborne throughout the entirety of the simulations. For the sake of clarity, twenty particles were sampled at random per expiration, for each of the three aerodynamic diameters (a total of 240 particles) and their track "tails" were mapped and visualized (Fig 10). Results suggested generally low particle travel distance between the point of injection into the model and the point of deposition. With the exception of a handful of distinct cases, the particles were injected and remained in the

9 ft span near the forward bulkhead where they either were continually re-entrained into the counter-rotating vortices around the side walls of the cabin or deposited onto a nearby surface. It should be noted that 0.1 µm and 1.0 µm particles were more likely to flow into the flight deck (Figs 10A and 10B). This was most likely due to their movement being dominated by airflow rather than gravitational forces. It was uncommon for all of the sizes and release times for particles to be transferred to the aircraft aft.

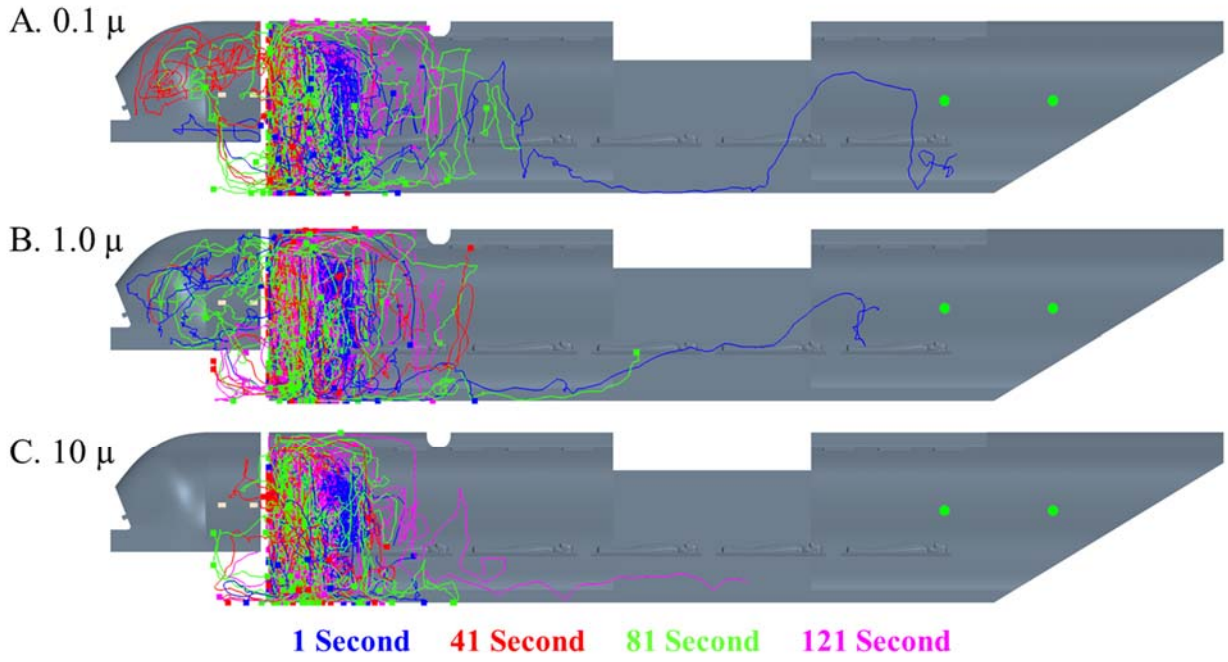

Figure 10 – Particle position tracking visualization
A. 20 × 0.1 µm particle tails for each of the release times; B. 20 × 1.0 µm particle tails for each of the release times; C. 20 × 10 µm particle tails for each of the release times.

4.3 Suspended Particle Velocity

While suspended, maximum particle velocity was recorded throughout the simulations. Results showed an initial 5-10 s period in all four simulations in which the expired particles briefly moved slowly, in the 0-5 ft/s range. As the particles began to disperse, they were entrained into the flow plumes originating from the overhead ventilation inlets in which they were accelerated sporadically to velocities as high as 41 ft/s (Figs 11A-D). Subsequently, the particles were pushed to vortices with lesser energy, and the maximum velocity leveled out at a magnitude of 20 ft/s.

Small discrepancies occurred between each expiration in the length of time in which the particles were continually re-energized. For instance, the predominant time period in which particles were re-energized for model 1 (1 s expiration) was between 20 s to 50 s, a 30 s duration (Fig 11A). Results were similar for models 2 and 4 (41 s and 121 s expiration) (Fig 11B, D). Results differed for model 3 (81 s expiration) as particles were energized for a much longer duration, from 90 s to 150 s, for a total of 60 s (Fig 11C).

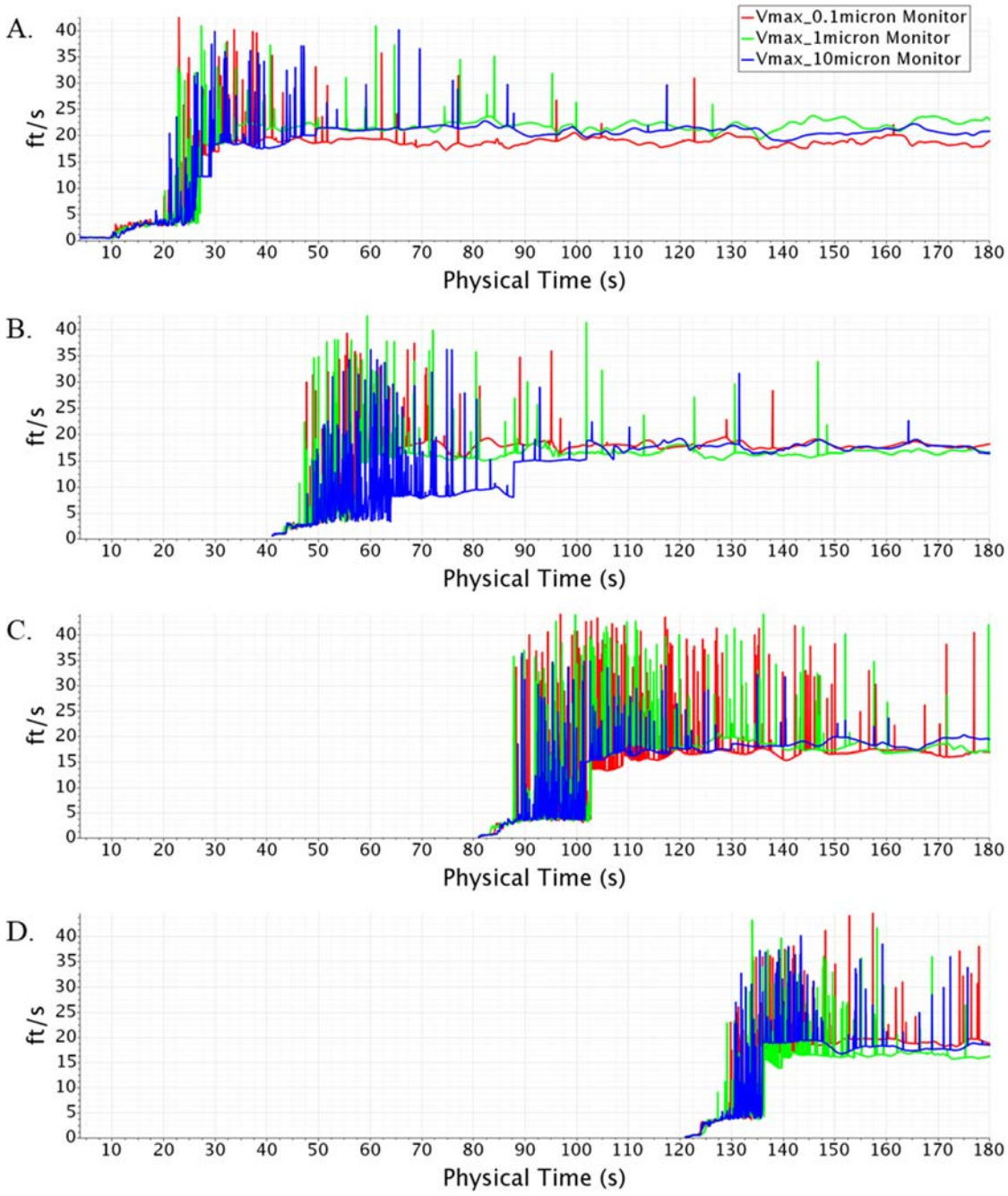

Figure 11 – Maximum particle velocity (Vmax) in time
A. Model 1 (1 s expiration); B. Model 2 (41 s expiration); C. Model 3 (81 s expiration); D. Model 4 (121 s expiration)

4.4 Particle Deposition

The approximately 100,000 particles per cough expiration were tracked for deposition and fate metrics throughout the 180 s simulations. At the 180 s mark, particles were located in one of three fates: still airborne, deposited to a surface or escaped through the ventilation outlets. All tracking plots followed the trend of initial expiration, brief suspension time before any

depositing or escaping, deposition and escape acceleration and an asymptotic approach to a single value (Fig 12).

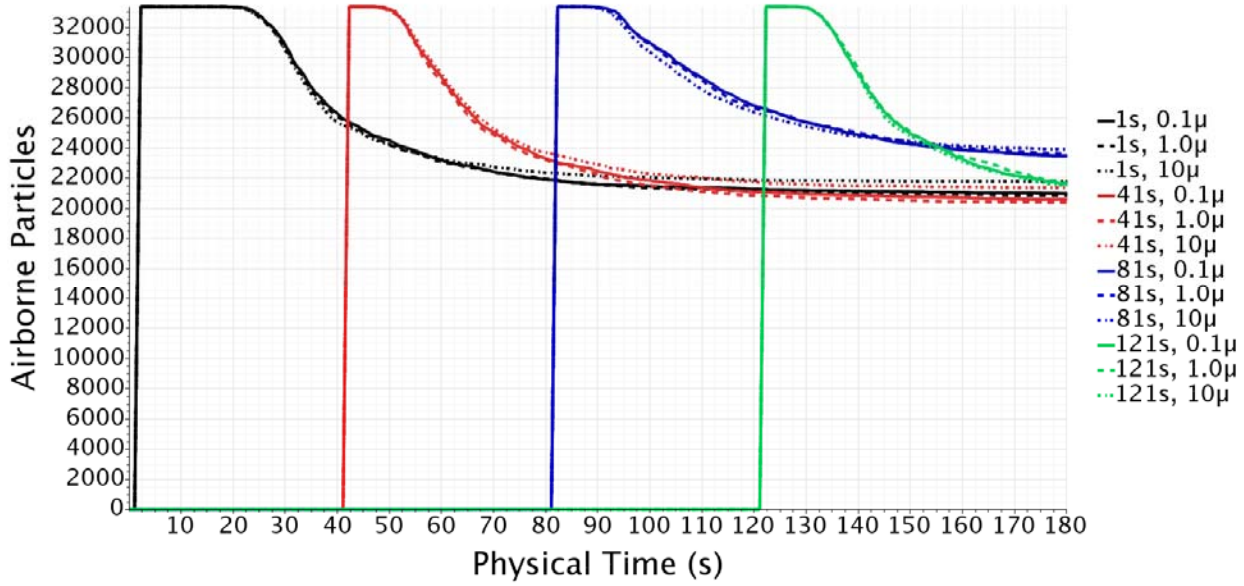

Figure 12 – Number of airborne particles suspended in the simulation over time

In each of the four models, the airborne particle count jumped from 0 to 33,333 per size per release over a period of 1.2 s. Subsequently, the particles were suspended for between 4 and 20 s before beginning to deposit or escape the domain. The longest residence time prior to particle deposit or escape occurred in model 1 (1 s expiration) for nearly 20 s, while the shortest was for 4 s in model 2 (41 s expiration). The residence time in models 3 (81 s expiration) and 4 (121 s expiration) was about 8 s prior to the initiation of any deposition or escape. Particle size had little effect on deposition and escape rates. The asymptotic decrease in airborne particle trends were similar in all four models; however, model 3 (81 s expiration) stood out as having the slowest rate of deposition and ultimate fate as well as approaching the highest asymptotic magnitude of all the cases, indicating it experienced the fewest deposited and escaped particles.

Particle numbers for each of the three fates (airborne, deposited and escaped) were investigated 50 s post initial deposition. The majority of particles remained suspended at the 50 s mark, followed by numbers of escaped and deposited. The average number of particles across all four models that remained suspended, deposited or escaped was 23,443 (70.3%), 2,085 (6.3%) and 7,805 (23.4%), respectively (Table 1). Values were very similar when scrutinizing the results from aerodynamic particle sizes discretely. The 0.1 µm particle averages were 23,377 (70.1%) suspended, 2,032 (6.1%) deposited and 7,924 (23.8%) escaped. The 1.0 µm particle averages were 23,380 (70.2%) suspended, 2,045 (6.1%) deposited and 7,908 (23.7%) escaped. The 10 µm particle averages were 23,573 (70.7%) suspended, 2,178 (6.5%) deposited and 7,582 (22.8%) escaped.

In all four models, the 10 micron size particles exhibited the highest deposition. However, the differences were relatively small. The total number of deposited particles per size were comparable for all cases, with the lowest being 1,710 and the highest being 2,396.

Table 1 – Particle Fate 50 Seconds Post Initial Deposition

Expiration	Particle Size	Airborne	Deposited	Escaped
1 s	0.1µ	22390	2071	8872
	1.0µ	22400	2055	8878
	10µ	22710	2168	8455
41 s	0.1µ	22830	2120	8383
	1.0µ	22540	2116	8677
	10µ	23370	2244	7719
81 s	0.1µ	25850	2227	5256
	1.0µ	26010	2288	5035
	10µ	25800	2396	5137
121 s	0.1µ	22440	1710	9183
	1.0µ	22570	1722	9041
	10µ	22410	1904	9019

Particles which adhered to the aircraft surfaces were further inspected for locational variation (Fig. 13). A total of 25,021 of the near 400,000 (6.3%) particles deposited throughout all four simulations. Particles deposited on beds 1-8 along with the flight deck floor and cargo door made up an extremely small fraction of the total 25,021 deposited particles (<1%). Particles adhered to the sidewalls more often than any other surface at 14,579 (58.3%), followed by the cargo floor at 6,719 (26.9%) and cargo rails at 2,214 (8.8%). The two litters closest to the point of expiration experienced the most deposited particles of the litters at 1,345 (5.4%). It should be noted that less than 60 particles (<0.2%) were found to deposit in the flight deck. Subtle trends occurred related to particle size, namely the frequency at which larger particles deposited on the horizontal surfaces and the smaller particles adhered to the sidewalls. In all cases, a slightly higher number of 10 µm particles deposited compared to the 0.1 µm and 1.0 µm sizes.

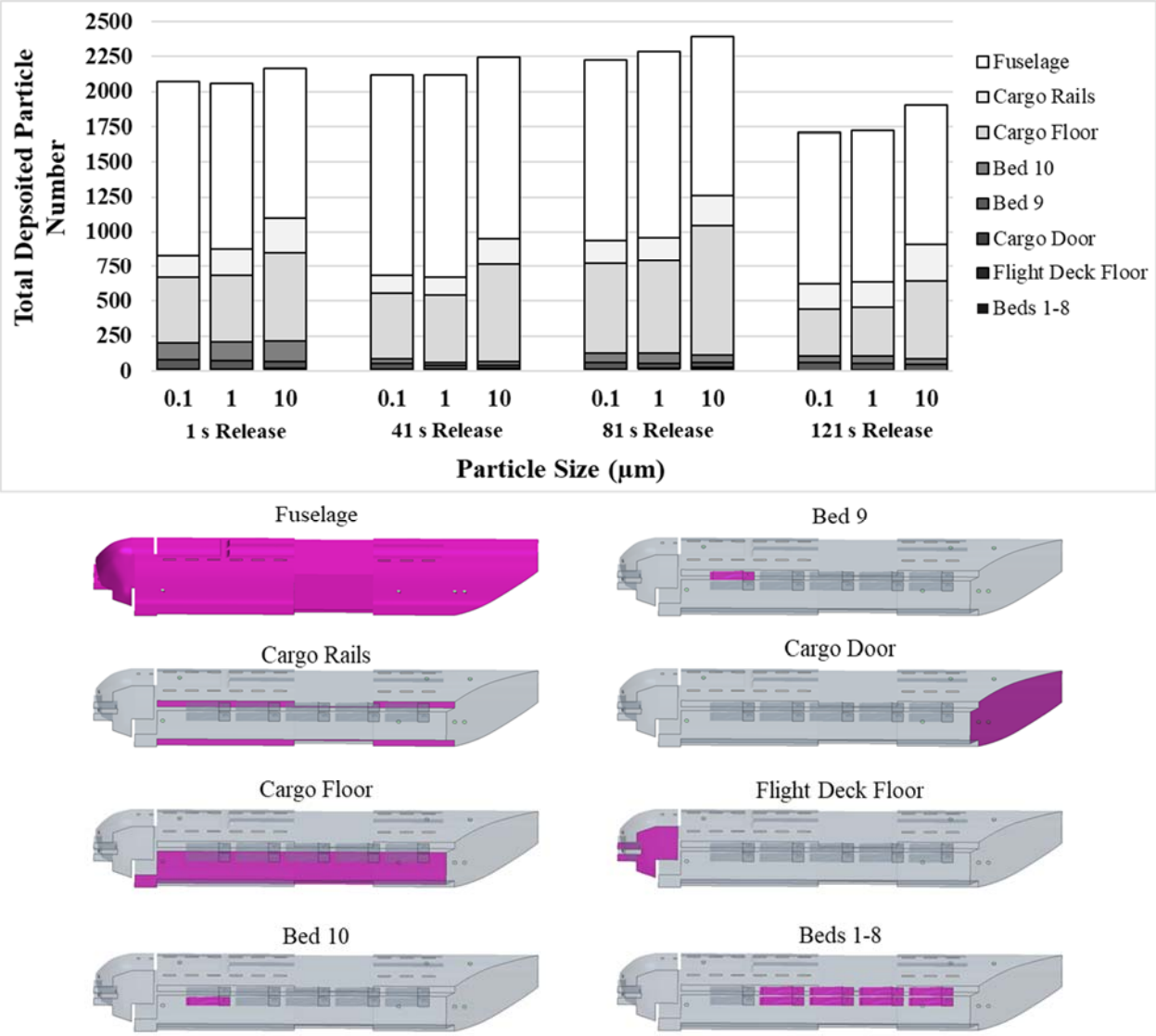

Figure 13 – Number of particles which adhered to each surface of interest

5.0 DISCUSSION

A series of four simulations were completed aboard a virtual C-130 in which 100,000 particles of three size ranges (0.1, 1.0 and 10 µm) were aerosolized using a standard cough profile at four different expiration times at 1, 41, 81 and 121 s. The typical CFD tool-chain was executed in which a C-130 cabin geometry was generated using laser scanning techniques, followed by volume meshing using polyhedral elements and physics application. A Reynolds-Averaged-Navier-Stokes with Lagrangian Multiphase scheme, 0.05 s time-step and first-order temporal discretization was used to resolve flow structures of air treated as an ideal gas.

Simulation results were investigated in a variety of manners including: air velocity direction and magnitude on six cut planes throughout the cabin, randomly sampled particle trajectories and their tails, single particle maximum velocities, particle deposition rates and particle locational binning. All investigations were in the transient state.

Air velocity investigation proved the flow to be unsteady with constant shedding, specifically in the 9 ft section of the cargo bay nearest the forward bulkhead (see Fig 8). Counter-rotating vortices developed and shed seemingly at random, originating at the ventilation inlets, traveling to the floor and turning direction to move upwards along the sidewalls (see Fig 9). Follow-on studies to further understand the flow dynamics require improved knowledge of the ventilation system design, as well as experimental validation.

Results showed that particles generally exhibited low travel distance from the point of expiration, which suggests that the location at which the particles are released into the aircraft cabin will play a strong role in their fate. Particle transport was dominated by the airflow physics, as none of the particles followed a ballistic trajectory in line with the simulated cough direction. Particles were quickly entrained into the velocity streams and dispersed near the point of release (see Fig. 10). Gupta et al. (2011a) also observed that airflow in a mockup commercial aircraft cabin was transient and dominated aerosol transport for 8.5 micron particles.

The time it took for the particles to become entrained into velocity streams varied from 20 to 60 s (see Fig. 11). The 60 s lag time corresponded to the third simulation where particles were released at 81 s (see Fig. 11C). Incidentally, this coincided with having the slowest rate of deposition and clearance and fewest deposited and escaped particles (see Fig. 12; Table 1, column 5). Therefore, slower deposition rates correlated to maximum particle velocity, indicating the particles entrained into higher-speed flow vortices were less likely to deposit or settle on a surface. A similar result was reported by Wan et al. (2009) in a computational study of bioaerosols in a mock aircraft cabin where small particles (< 28 microns) primarily remained entrained in airflow and particle deposition decreased with increased airflow velocity.

After the initial deposition period, airborne particles approached an asymptotic value, indicating the potential for significant accumulation and airborne superposition of suspended particles with recurring expiration events. These results are in agreement with work completed by Gupta et al. which concluded that droplet movement was governed by bulk airflow after the discharge and droplets followed similar trajectories independent of discharge time (Gupta et al., 2011a).

Particle fate for each of the three particle sizes varied minimally in each of the four models (see Table 1). This indicates that unsteady flow eddies affected overall fate minimally. The majority of all particles (70.3% on average) remained suspended for the duration of the simulations, while a smaller percentage escaped through the ventilation outlets (23.4% on average). Only 6.3% of the particles deposited to cabin surfaces on average. These results were consistent with previous studies, which have shown that small droplet nuclei (< 20 μm) can remain suspended in air currents for prolonged periods of time (Morawska, 2006).

Deposition patterns were consistent across all the expiration events in which the surfaces nearest the expiration experienced the greatest deposition magnitudes (see Fig. 13). Particles adhered to the cabin sidewalls more often than any other surface (58.3%) followed by the cargo floor (26.9%). The 10.0 μm particles were 1.46 times more likely than the 0.1 and 1.0 μm particles to settle on horizontal surfaces, while 0.1 to 1.0 μm particles were 1.12 times more likely to adhere to the sidewalls and patients, which is in agreement with a study completed by Wan et al. (2009) in which the results suggested that aerosol deposition fraction increased with aerodynamic diameter. This result is expected due to the greater gravitational influence for larger particles.

6.0 CONCLUSIONS AND FUTURE WORK

In conclusion, a preliminary numerical study showed the viability of using Lagrangian Multiphase simulation techniques to predict bioaerosol transport, residence time, deposition and clearance aboard a military cargo aircraft. The study demonstrated a proof-of-concept approach for investigating the correlation between airflow mechanics and aerosol distribution based on CFD output. These findings show that ventilation flow patterns were favorable to keep aerosols suspended for an extended duration. Infection risk due to inhalation of suspended microorganism-bearing droplets between 0.1 and 10 μm was 10 times higher than the risk due to surface contact. Further, after the initial deposition period, airborne particles approached an asymptotic value, indicating the potential for significant accumulation and superposition of suspended particles with recurring expiration events. Based on the results of this preliminary study, decontamination and sampling procedures should focus on the vicinity in which the infected passenger was located, primarily on the sidewalls.

Plans to validate this work are in place and will be executed via sampling methods aboard operational C-130 aircraft. Polystyrene latex spheres of different biologically-relevant size distributions will be aerosolized using parameters to best mimic real-world conditions. Aerosol samplers (i.e., active and passive samplers), such as the Instantaneous Biological Analyzer and Collector (IBAC), passive deposition filters, three-button aerosol samplers and nanoparticle detectors will be employed throughout the aircraft. The simulation setup will be recreated during flight in which an aerosol will be generated and released near the forward bulkhead and tracked using the active and passive sampling methods previously stated. Computational and experimental results will be compared to instigate further improvement on model accuracy.

REFERENCES

Centers for Disease Control and Prevention (CDC). 2005. Guidelines for Preventing the Transmission of *Mycobacterium tuberculosis* in Health-Care Settings. Morbidity and Mortality Weekly Report, Vol. 54, No. RR-17.

Chao, C.Y.H.; M.P. Wan; L. Morawska; G.R. Johnson; Z.D. Ristovski; M. Hargreaves; K. Mengersen; S. Corbett; Y. Li; X. Xie; D. Katoshevski. 2009. Characterization of expiration air jets and droplet size distributions immediately at the mouth opening. Aerosol Science 40:122-133.

Crowhurst, J.W. Air Force Instruction 11-2AE Volume 3, Addenda-A. Aeromedical Evacuation Operations Configuration/Mission Planning. Updated 17 May 2011.

Elmaghraby, H.A.; Y.W. Chiang, A.A. Aliabadi. 2018. Ventilation strategies and air quality management in passenger aircraft cabins: A Review of experimental approaches and numerical simulations. Science and Technology for the Built Environment 24(2):160–175.

Fabian, P.; J.J. McDevitt; W.H. DeHaan; R.O. Fung; B.J. Cowling; K.H. Chan; G.M. Leung; D.K. Milton. 2008. Influenza virus in human exhaled breath: An observational study. PLoS ONE 3(7):e2691.

Fernstrom, A.; M. Goldblatt. 2013. Aerobiology and its role in the transmission of infectious diseases. Journal of Pathogens 2013:ArticleID493960 (13 pages).

Frankel, M.; G. Bekö; M. Timm; S. Gustavsen; E.W. Hansen; A.M. Madsen. 2012. Seasonal variations of indoor microbial exposures and their relation to temperature, relative humidity, and air exchange rate. Applied and Environmental Microbiology 78(23):8289–8297.

Gupta, J. K.; C.-H. Lin; Q. Chen. 2010. Prediction of spatial and temporal distribution of expiratory droplets in an aircraft cabin. International High Performance Buildings Conference.

Gupta, J.K.; C.-H. Lin; Q. Chen. 2011a. Transport of expiratory droplets in an aircraft cabin. Indoor Air 21(1):3–11.

Gupta, J.K.; C.-H. Lin; Q. Chen. 2011b. Inhalation of expiratory droplets in aircraft cabins. Indoor Air 21(4):341–350.

Hocking, M.B. 1998. Indoor air quality: Recommendations relevant to aircraft passenger cabins. American Industrial Hygiene Association Journal 59:446–454.

Lindsley, W.G.; F.M. Blachere; R.E. Thewlis; A. Vishnu; K.A. Davis; G. Cao; J.E. Palmer; K.E. Clark; M.A. Fisher; R. Khakoo; D.H. Beezhold. 2010. Measurements of airborne influenza virus in aerosol particles from human coughs. PLoS One 5(11):e15100.

Lindsley, W.G.; J.S. Reynolds; J.V. Szalajda; J.D. Noti; D.H. Beezhold. 2013. A cough aerosol simulator for the study of disease transmission by human cough-generated aerosols. Aerosol Science and Technology 47(8):937–944.

Lockheed Martin Aeronautics Company. C-130J Super Hercules Pocket Guide. A12-37957A001. Available from: https://lockheedmartin.com/content/dam/lockheed-martin/aero/documents/C-130J/C130JPocketGuide.pdf.

Morawska, L.; G.R. Johnson; Z.D. Ristovski; M. Hargreaves; K. Mengersen; S. Corbett; C.Y.H. Chao; Y. Li; D. Katoshevski. 2009. Size distribution and sites of origin of droplets expelled from the human respiratory tract during expiratory activities. Journal of Aerosol Science 40:256–269.

Morawska, L. 2006. Droplet fate in indoor environments, or can we prevent the spread of infection? Indoor Air 16:335-347.

Nardell, E.A. 1990. Dodging droplet nuclei: Reducing the probability of nosocomial tuberculosis transmission in the AIDS era. The American Review of Respiratory Disease 142:501–503.

Stelzer-Braid, S.; B.G. Oliver; A.J. Blazey; E. Argent; T.P. Newsome; W.D. Rawlinson; E.R. Tovey. 2009. Exhalation of respiratory viruses by breathing, coughing, and talking. Journal of Medical Virology 81:1674–1679.

Sze To, G.N.; M.P. Wan; C.Y.H. Chao; L. Fang; A. Melikov. 2009. Experimental study of dispersion and deposition of expiratory aerosols in aircraft cabins and impact on infectious disease transmission. Aerosol Science and Technology 43(5):466–485.

U.S. Air Force. C-130 Hercules. “C-130 Hercules.” Photo taken 15 March 2018, Available from: www.af.mil/About-Us/Fact-Sheets/Display/Article/1555054/c-130-hercules/.

U.S. Air Force. Air Force Photos. “Aeromedical Evacuation Missions: behind the Scenes.” Photo taken 20 July 2013, Available from: www.af.mil/News/Photos/igphoto/2000704785/.

Wan, M.P.; G.N. Sze To; C.Y.H. Chao; L. Fang; A. Melikov. 2009. Modeling the fate of expiratory aerosols and the associated infection risk in an aircraft cabin environment. Aerosol Science and Technology 43(4):322–343.

Withers, M.R.; G.W. Christopher. 2000. Aeromedical Evacuation of Biological Warfare Casualties: Aeromedical Evacuation of Biological Warfare Casualties: A Treatise on Infectious Diseases on Aircraft. U.S. Military Medicine.

Zhai, S.; Z. Li; B. Zhao. 2014. State-space analysis of influencing factors on airborne particle concentration in aircraft cabins. Building and Environment 74:13–21.

ABBREVIATIONS

AE	Aeromedical Evacuation
AF	Air Force
CAD	Computer Aided Design
CFD	Computational Fluid Dynamics

APPENDIX A
Faro Scan Results

Top-down view of C-130H point cloud showing scan locations as blue dots. Note the number of scans required for proper flight deck resolution. 16 point-cloud scans were registered to a single, comprehensive geometry of the C-130H cabin, including the cargo bay and flight deck. The point cloud was used to take virtual measurements of the domain and create and analogous solid model.

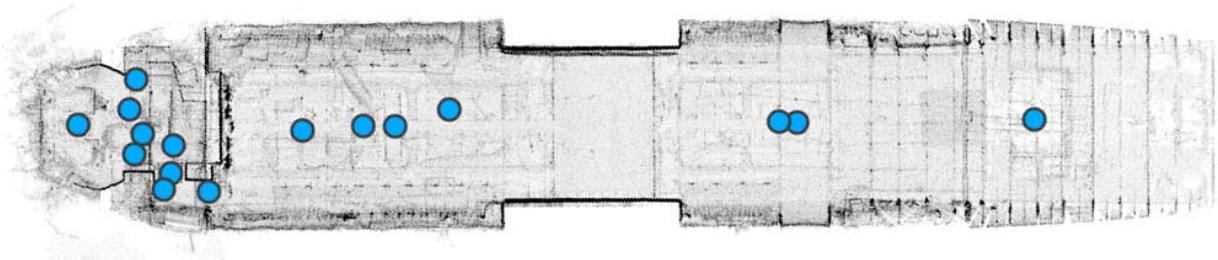

Figure A1 – C-130 point cloud scan locations

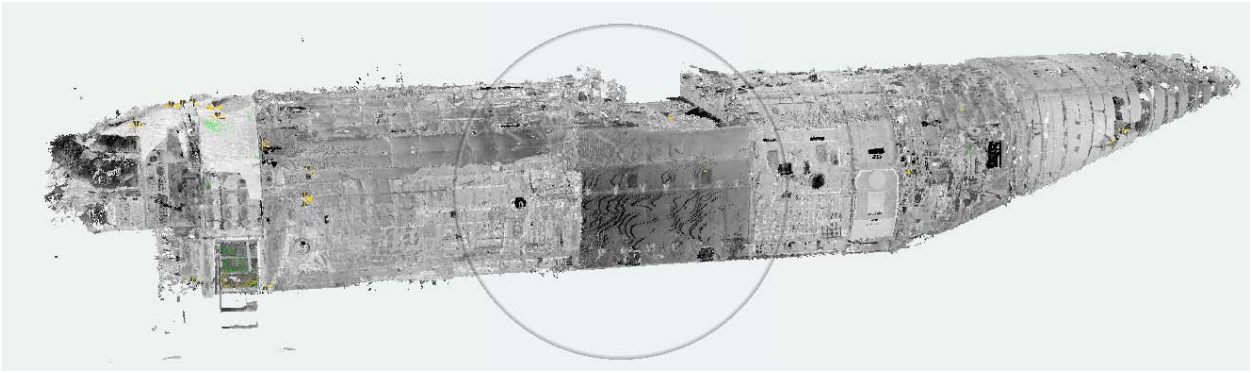

Figure A2 – Fully registered software-generated C-130H point cloud

APPENDIX B.

Air Velocity from Forward to Aft on Investigation Planes throughout the Aircraft Cabin

Airflow dynamics were scrutinized at four time points 4 s apart starting at 9-19 s after the initial particle release in each of the four models due to the association of this time period with high frequency particle deposition. When visualized on plane 6 (see Fig. 7 for definition), the first model (particle release at 1 s) showed much of the air flowing from forward to aft (positive flow, red) at a magnitude between 0.0 and 0.5 ft/s near the mid-section of the aircraft and negative flow (blue) near the bulkhead (see Fig. 8). This result was also observed in the other three models where particles were released at 41 s, 81 s and 121 s (Fig. B1-3).

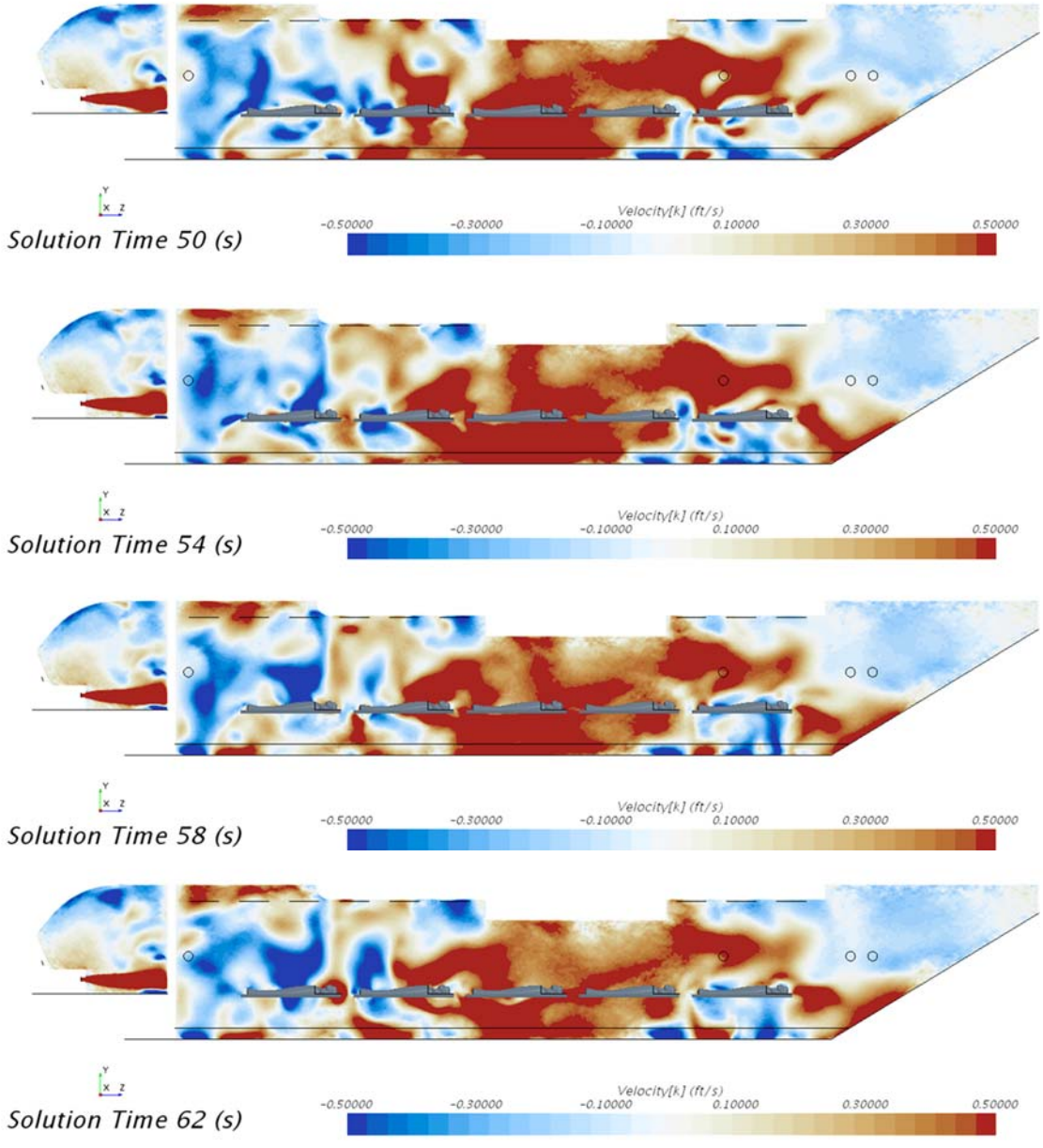

Figure B1 – Air velocity in forward to aft direction on plane 6 in model 2

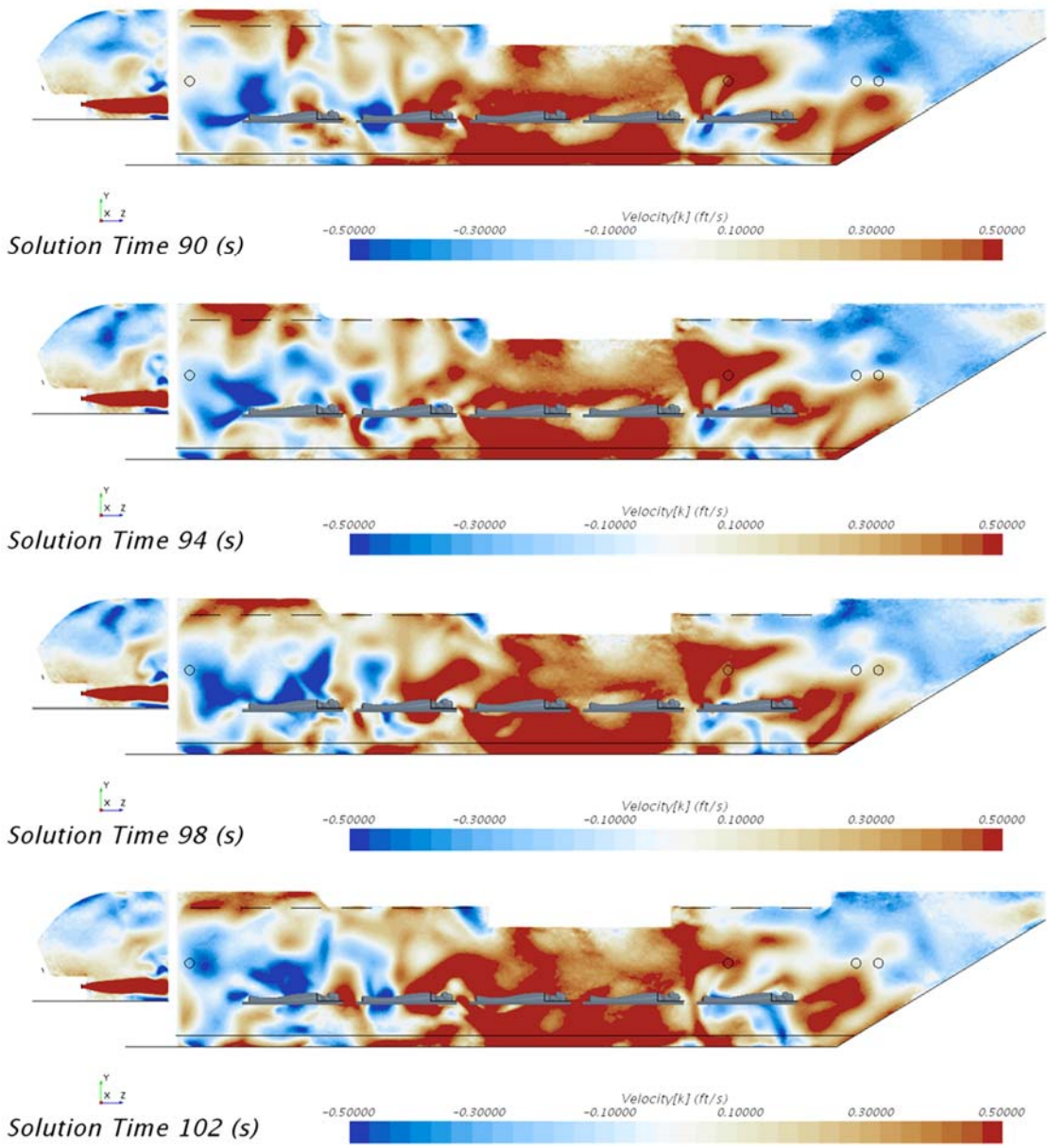

Figure B2 – Air velocity in forward to aft direction on plane 6 in model 3

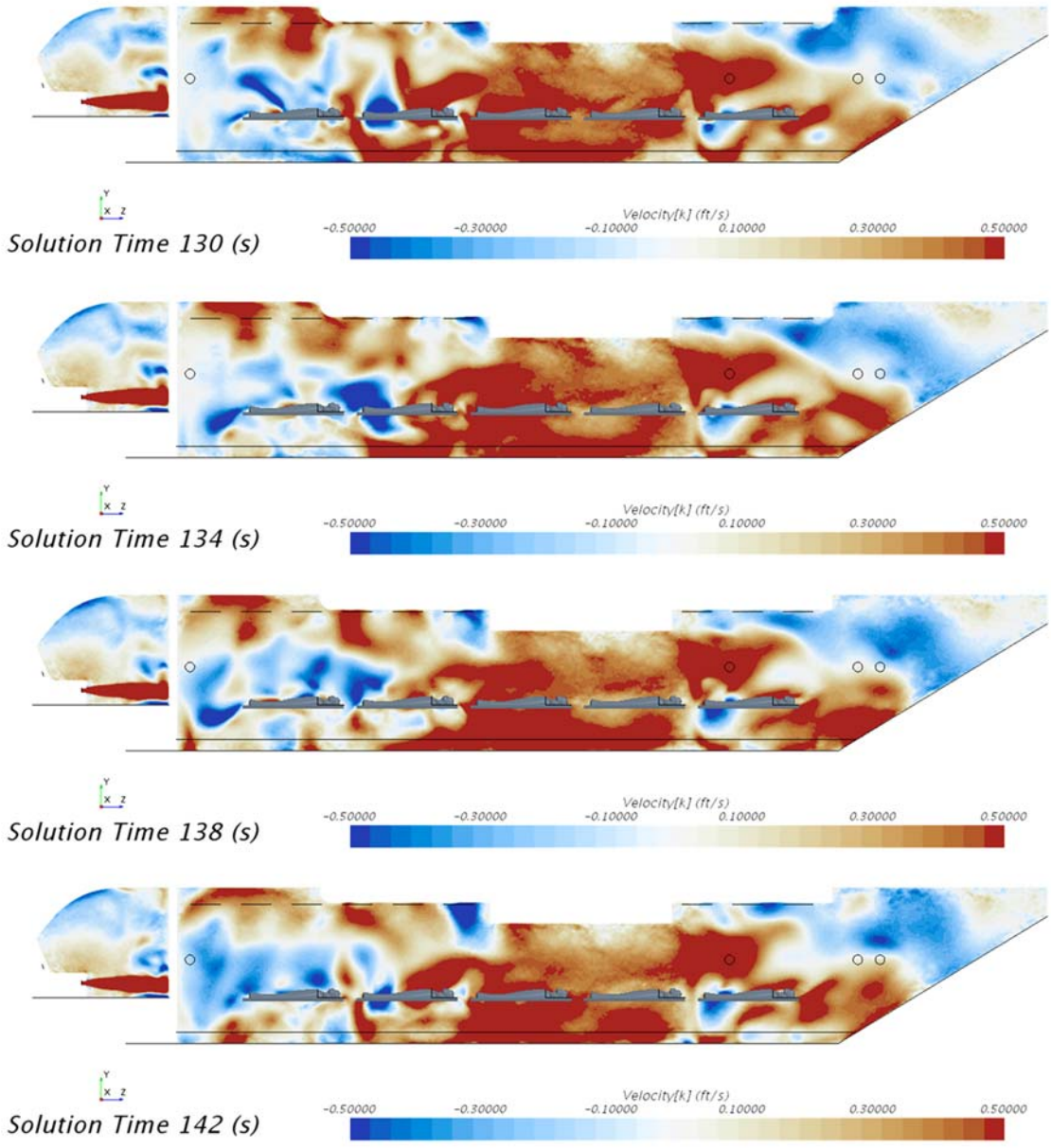

Figure B3 – Air velocity in forward to aft direction on plane 6 in model 4

Planes 1-5 showed similar results along cut planes perpendicular to plane 6 and parallel to the forward bulkhead (summarized in Fig. 9). Flow was perceived to exhibit transient flow structures in a combination of positive and negative flow in the forward to aft direction. Flow direction variation was high in all temporal and locational snapshots; however, negative flow was more commonly observed at the center of planes 1-5 and along the floor of the aircraft whereas positive flow occurred around the perimeter of the same cut planes. The snapshots at each of the four time points starting 19 s after the initial particle release in each of the four models on each of the five axial cut planes are shown in Figures B4-8. See Figure 7 for a diagram showing the location of each cut plane.

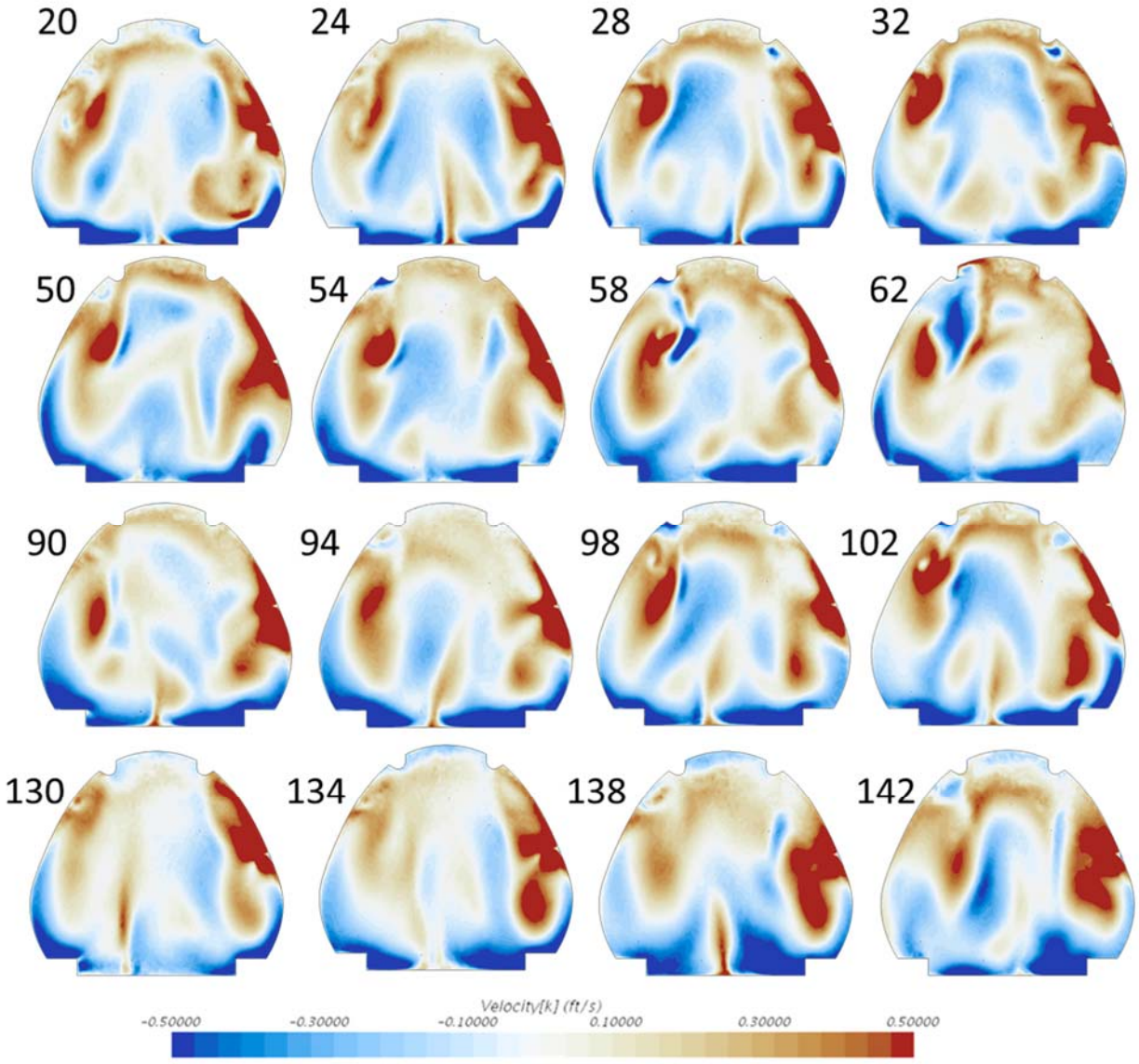

Figure B4 – Air velocity in forward to aft direction on plane 1 in models 1-4

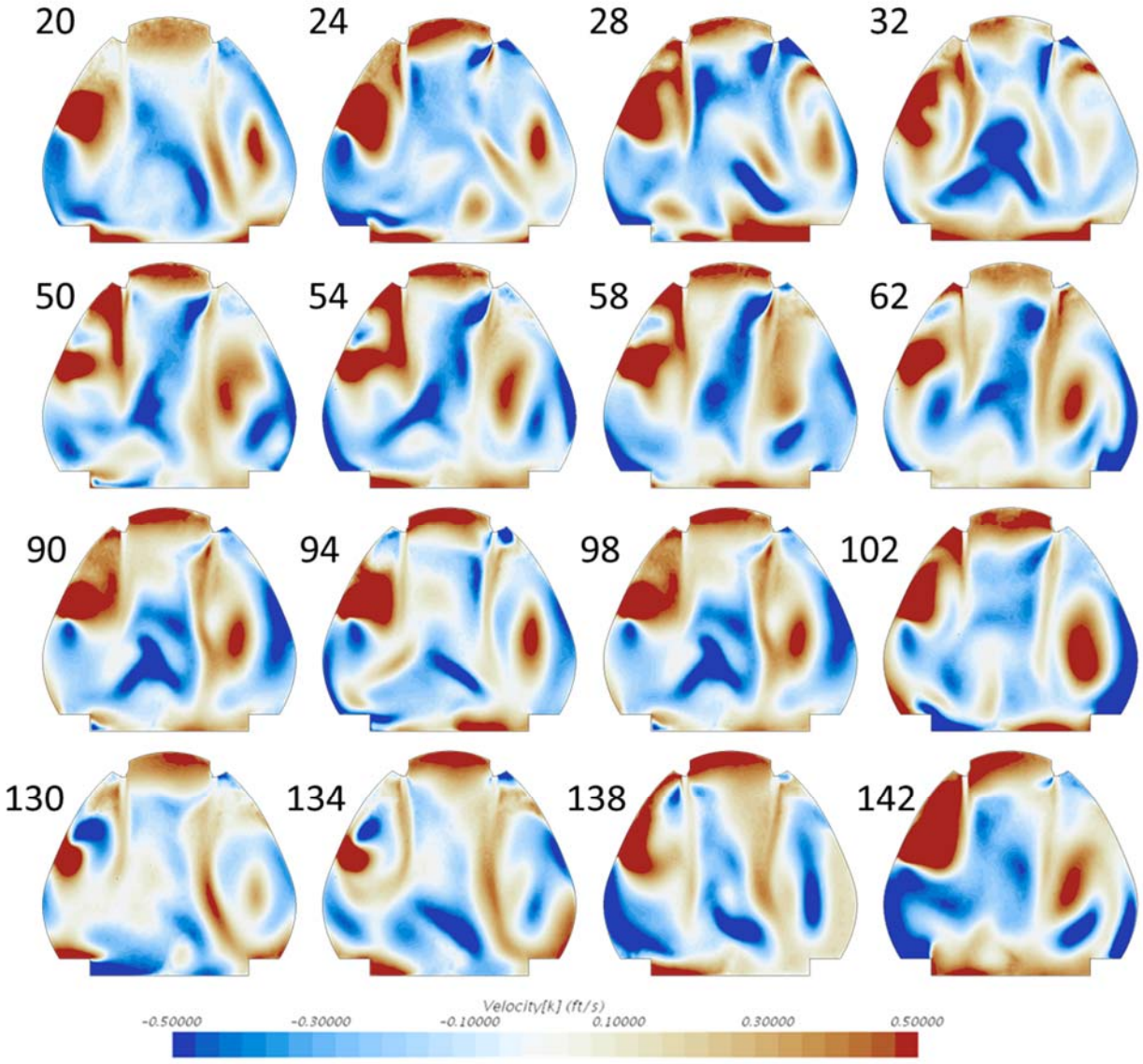

Figure B5 – Air velocity in forward to aft direction on plane 2 in models 1-4

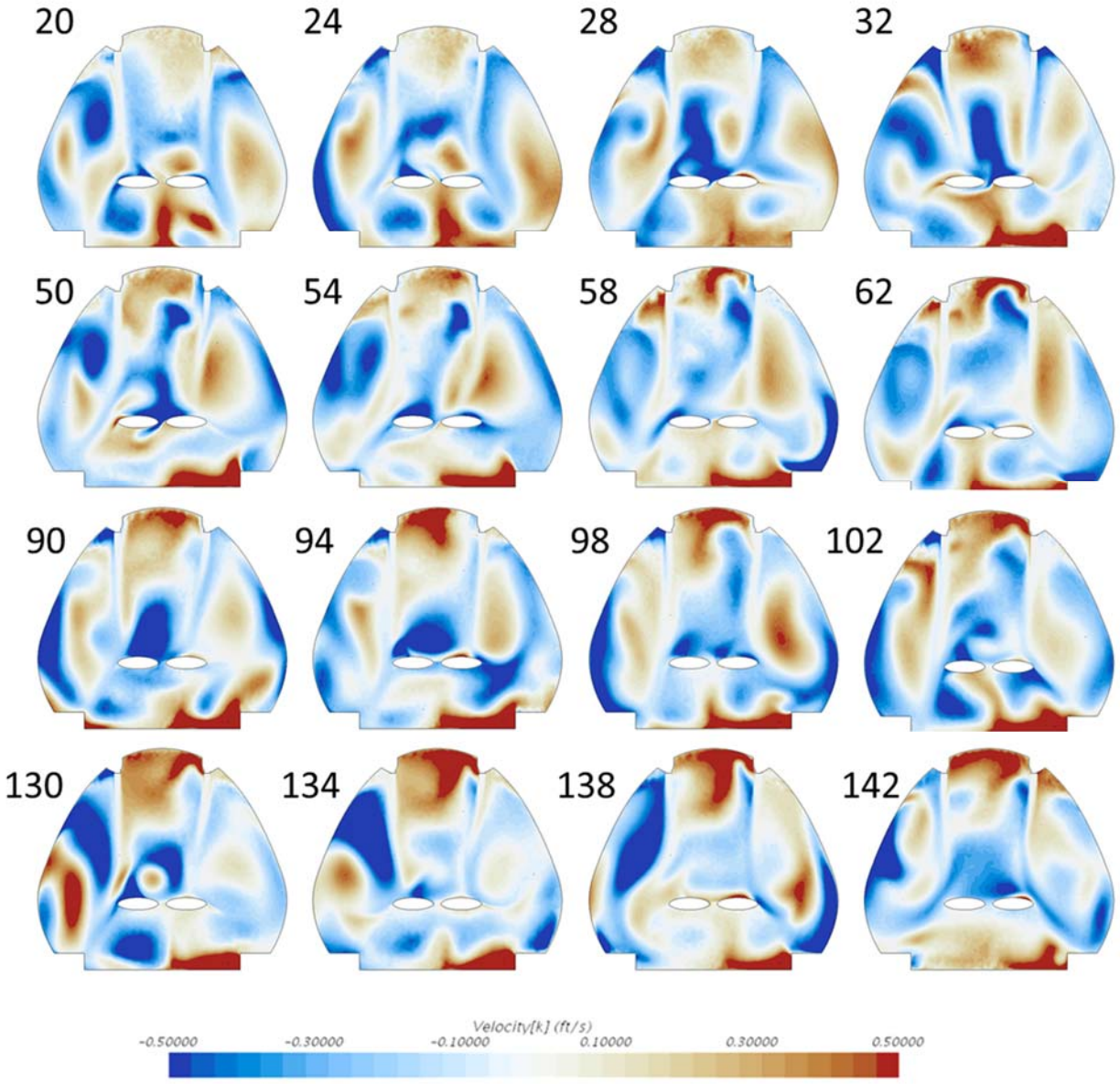

Figure B6 – Air velocity in forward to aft direction on plane 3 in models 1-4

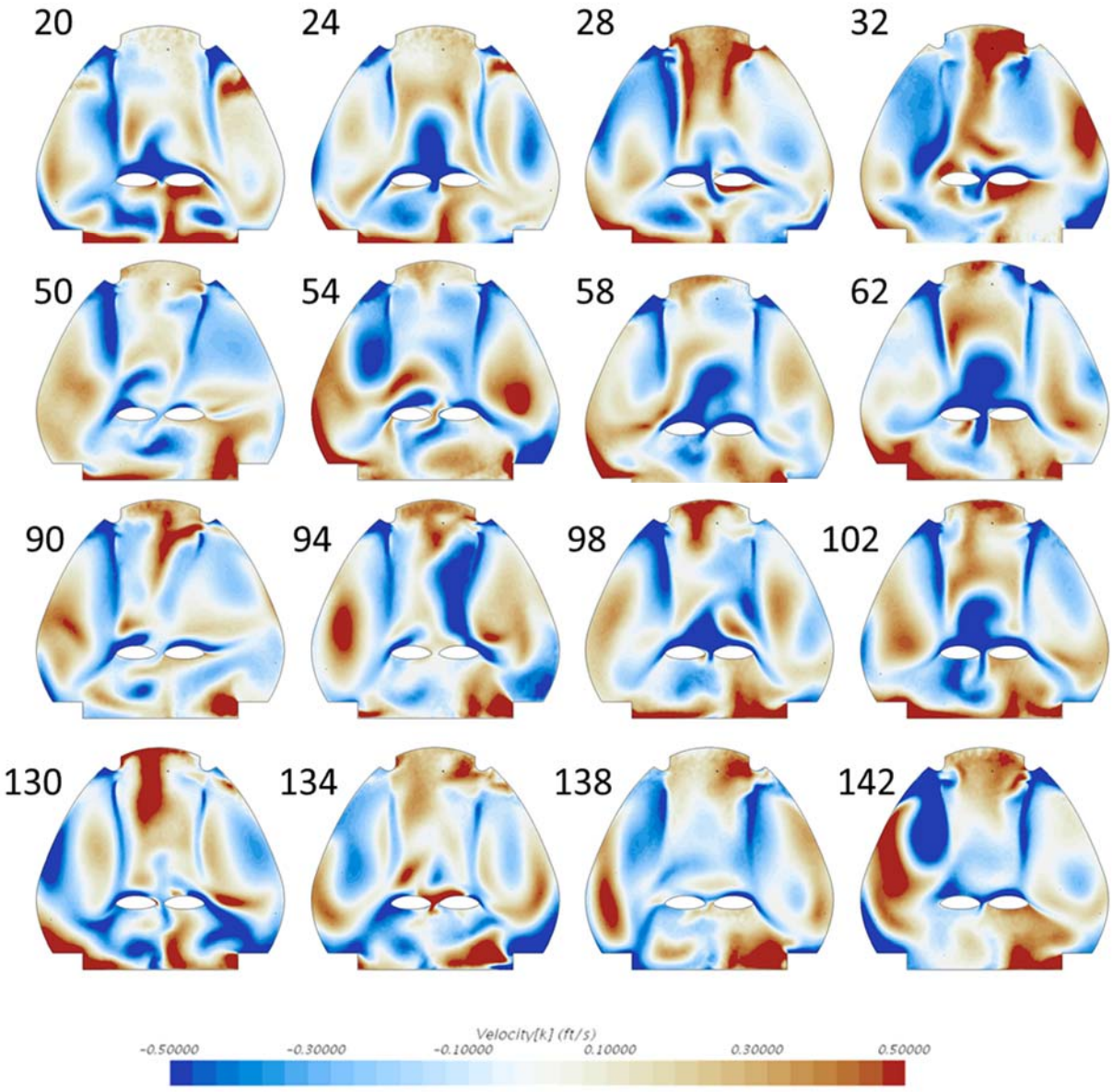

Figure B7 – Air velocity in forward to aft direction on plane 4 in models 1-4

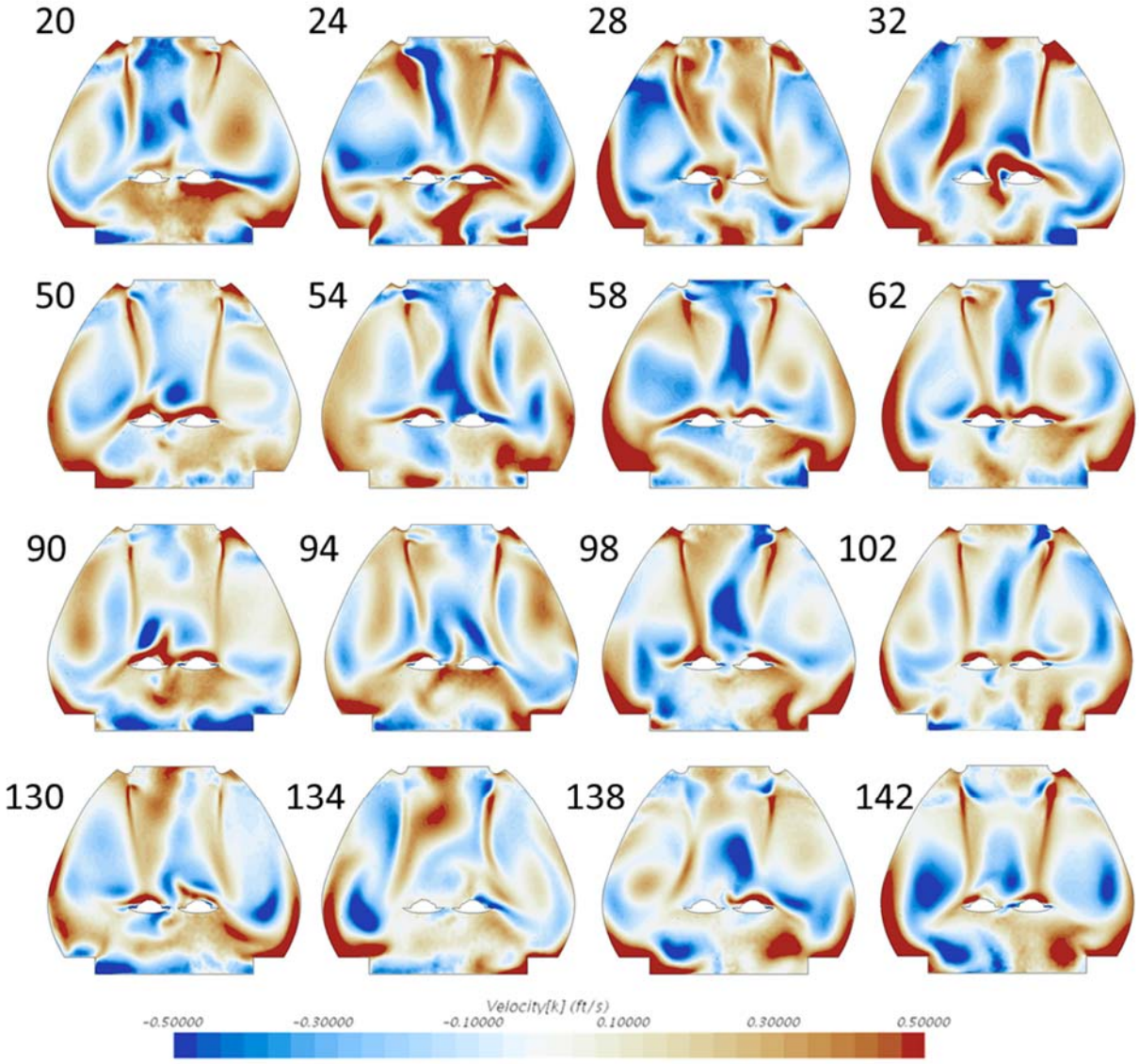

Figure B8 – Air velocity in forward to aft direction on plane 5 in models 1-4

APPENDIX C
Visualized Deposition Patterns for each of the Four Models

Particles deposited most frquently across the forward section of the cargo bay in all four models (expirations at 1, 41, 81 and 121 s for models 1, 2, 3 and 4, respectively). The following figures depict the locations of deposition which are clustered around the aerosol expiration point.

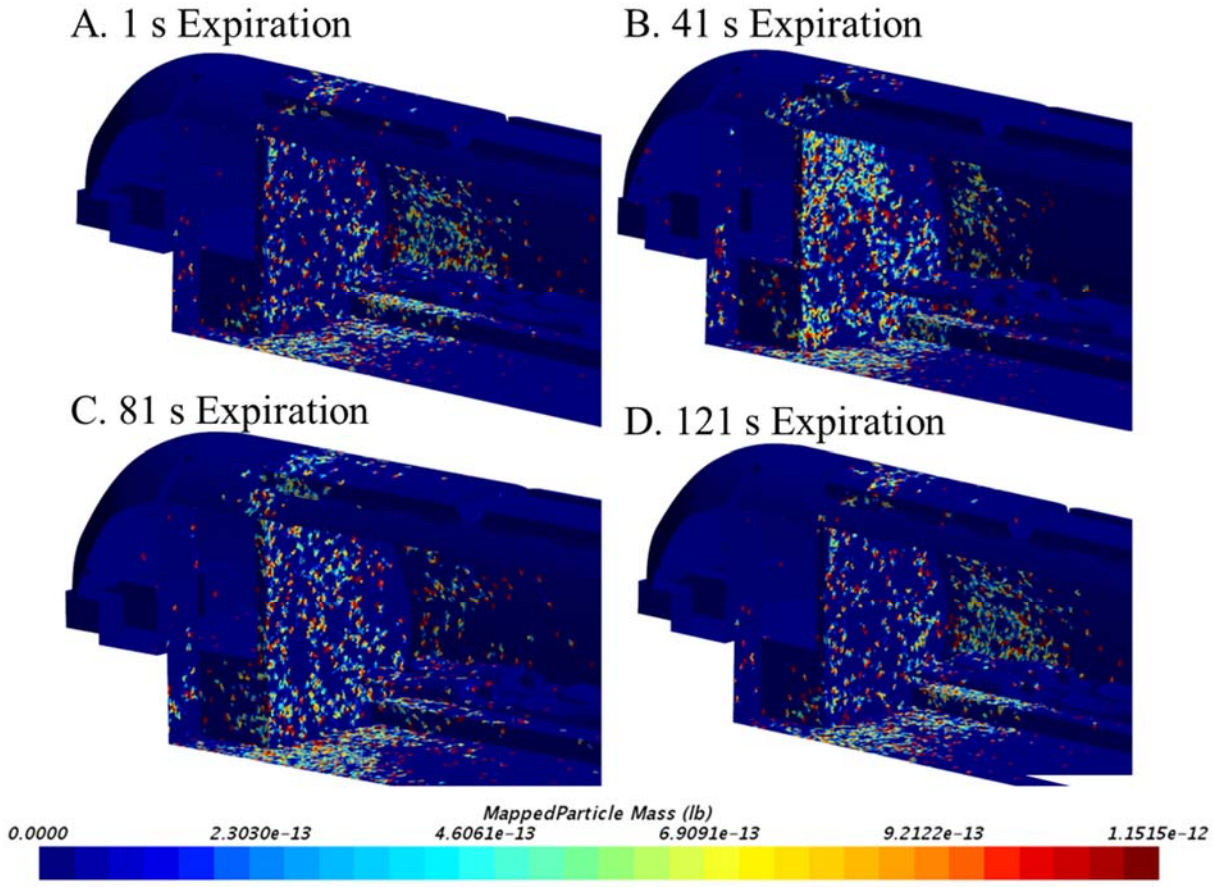

Figure C1 – Detailed particle deposition patterns by mass for each of the four models
A. model 1; B. model 2; C. model 3; D. model 4